Published in final edited form as:

Cell Signal. 2016 September ; 28(9): 1364–1379. doi:10.1016/j.cellsig.2016.06.012.

Soluble guanylyl cyclase-activated cyclic GMP-dependent protein kinase inhibits arterial smooth muscle cell migration independent of VASP-Serine 239 phosphorylation

Andrew W. Holt[1], **Danielle N. Martin**[1], **Patti R. Shaver**[2], **Shaquria P. Adderley**[1], **Joshua D. Stone**[1], **Chintamani N. Joshi**[1], **Jake T. Francisco**[1], **Robert M. Lust**[1], **Douglas A. Weidner**[3], **Brian M. Shewchuk**[2], and **David A. Tulis**[1,*]

[1]Department of Physiology, Brody School of Medicine, East Carolina University, Greenville, NC

[2]Department of Biochemistry, Brody School of Medicine, East Carolina University, Greenville, NC

[3]Department of Microbiology and Immunology, Brody School of Medicine, East Carolina University, Greenville, NC

Abstract

Coronary artery disease (CAD) accounts for over half of all cardiovascular disease-related deaths. Uncontrolled arterial smooth muscle (ASM) cell migration is a major component of CAD pathogenesis and efforts aimed at attenuating its progression are clinically essential. Cyclic nucleotide signaling has long been studied for its growth-mitigating properties in the setting of CAD and other vascular disorders. Heme-containing soluble guanylyl cyclase (sGC) synthesizes cyclic guanosine monophosphate (cGMP) and maintains vascular homeostasis predominantly through cGMP-dependent protein kinase (PKG) signaling. Considering that reactive oxygen species (ROS) can interfere with appropriate sGC signaling by oxidizing the cyclase heme moiety and so are associated with several CVD pathologies, the current study was designed to test the hypothesis that heme-independent sGC activation by BAY60-2770 (BAY60) maintains cGMP levels despite heme oxidation and inhibits ASM cell migration through phosphorylation of the PKG target and actin-binding vasodilator-stimulated phosphoprotein (VASP). First, using the heme oxidant ODQ, cGMP content was potentiated in the presence of BAY60. Using a rat model of arterial growth, BAY60 significantly reduced neointima formation and luminal narrowing compared to vehicle (VEH)-treated controls. In rat ASM cells BAY60 significantly attenuated cell migration, reduced G:F actin, and increased PKG activity and VASP Ser239 phosphorylation

*Corresponding author: David A. Tulis (tulisd@ecu.edu); Department of Physiology, 600 Moye Boulevard, Brody School of Medicine, East Carolina University, Greenville, NC 27834; Phone: 252-744-2771.

Conflict of interest discloser

None

Authors' contributions

AWH, SPA, CNJ, and DAT conceived the study. AWH, DNM, SPA, JDS, CNJ, JTF, DAW, and DAT carried out the experiments and performed statistical analyses. RML performed the vascular ultrasound experiments and BMS designed and PS created the site-directed mutagenesis constructs. AWH, DNM and DAT drafted the manuscript. All authors contributed to the revision and approval of the final manuscript.

(pVASP.S239) compared to VEH controls. Site-directed mutagenesis was then used to generate overexpressing full-length wild type VASP (FL-VASP/WT), VASP Ser239 phosphorylation-mimetic (FL-VASP/ 239D) and VASP Ser239 phosphorylation-resistant (FL-VASP/239A) ASM cell mutants. Surprisingly, FL-VASP/239D negated the inhibitory effects of FL-VASP/ WT and FL-VASP/239A cells on migration. Furthermore, when FL-VASP mutants were treated with BAY60, only the FL-VASP/239D group showed reduced migration compared to its VEH controls. Intriguingly, FL-VASP/239D abrogated the stimulatory effects of FL-VASP/WT and FL-VASP/239A cells on PKG activity. In turn, pharmacologic blockade of PKG in the presence of BAY60 reversed the inhibitory effect of BAY60 on naïve ASM cell migration. Taken together, we demonstrate for the first time that BAY60 inhibits ASM cell migration through cGMP/PKG/VASP signaling yet through mechanisms independent of pVASP.S239 and that FL-VASP overexpression regulates PKG activity in rat ASM cells. These findings implicate BAY60 as a potential pharmacotherapeutic agent against aberrant ASM growth disorders such as CAD and also establish a unique mechanism through which VASP controls PKG activity.

Graphical Abstract

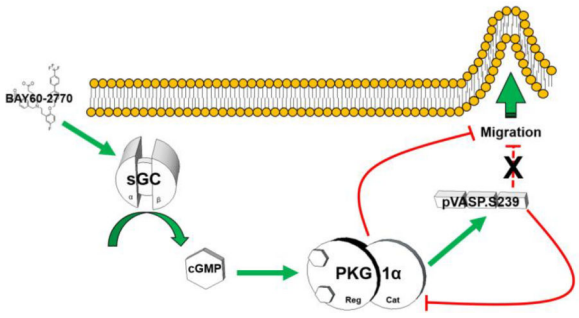

Keywords

BAY 60-2770; cGMP; migration; PKG; smooth muscle cell; VASP

1. Introduction

Coronary artery disease (CAD) accounts for over half of all cardiovascular disease-related deaths [1]. Like many vascular pathologies, CAD is characterized by matrix imbalance, pathologic arterial smooth muscle (ASM) proliferation and migration and a heightened immune response [1]. Intriguingly, soluble guanylyl cyclase (sGC) expression and cyclic GMP-dependent protein kinase (PKG) activity are depressed while reactive oxygen species (ROS) are elevated following vascular injury or disease. In turn, these events have been speculated to contribute to dysfunctional homeostatic cell signaling linked to atherogenesis, ASM cell hyperplasia and vessel wall hypertrophy, luminal narrowing, and phenotypic switching from a contractile to synthetic, pro-growth phenotype [2–4]. Importantly, canonical sGC function requires a reduced heme moiety within its two heterodimeric subunits [5]. Because reactive oxygen species (ROS) are a risk factor for CVD pathologies, ROS-mediated oxidation of the sGC heme iron prevents NO binding and negatively impacts homeostatic cell signaling which has been found to promote aberrant ASM growth [5,6]

Additionally, current surgical strategies include balloon angioplasty and/or stent deployment which often fail due to vessel remodeling and neointimal development [7]. The current study was designed to investigate ability of pharmacologic heme-independent activation of endogenous sGC to prevent ASM cell migration as a key component of pathologic vascular growth.

The principal cardiovascular effects of carbon monoxide (CO) and NO are facilitated through activation of sGC with subsequent synthesis of second messenger cGMP. Together, CO/NO and cGMP serve key protective roles in cardiovascular disorders associated with its regulation of vasomotor tone, cell adhesion to endothelium, inhibition of platelet aggregation, and ASM cell proliferation and migration [8–12]. A well-characterized downstream effector target of cGMP within the vasculature is PKG1 [13–15].

PKG1 is a serine (Ser)/threonine (Thr) kinase that exists as two isoforms, PKG1α and 1β, which are formed through alternative splicing of the N-terminus of the PKG1 gene and which dose-dependently respond to cGMP in the vasculature [16]. Through post-translational phosphorylational control, PKG is centrally involved in regulating intracellular on/off switches that help control manifold cellular processes including inhibition of calcium mobilization and phosphorylation of the small heat shock-related protein (Hsp) 20 to promote vascular dilation [17]. Previous studies have shown capacity of traditional modes of PKG activation to modulate arterial growth [18–21], yet many of these elicit off-target hypotensive effects in the clinical setting [22] and thereby warrant identification and characterization of alternate approaches for cGMP/PKG stimulation as well as more discrete ASM targets.

Notably, PKG preferentially phosphorylates the actin-binding, focal adhesion adaptor vasodilator-stimulated phosphoprotein (VASP) which has been proposed instrumental in modulating cellular migration [23–25]. The critical role for VASP in actin-mediated migration makes it an attractive target for whole vessel- and ASM-directed therapies. Regarding cyclic nucleotide-mediated downstream effectors, VASP is a well-characterized Ser/Thr kinase substrate that was identified after researchers recognized discrete phosphorylation sites at Ser239 and Ser157 after treating cells with cGMP and cAMP agonists, respectively [26]. Over time, VASP has gained notoriety in terms of its unique phosphorylation status and its proposed involvement as a regulator of cell migration and motility [23,27,28]. VASP has been cited in over forty clinical trials where it is predominantly used as a readout in platelet aggregation studies, and cell signaling experiments routinely use phosphorylated VASP at Ser239 (pVASP.S239) and/or Ser157 (pVASP.S157) to indirectly measure PKG/PKA activities [29–31]. Nonetheless, pVASP.S239 has not yet been examined as a therapeutic target in vascular growth disorders nor has it been explored as an independent mechanism for sGC-mediated therapies. The present study was performed to test our hypothesis that the heme-independent sGC activator BAY 60-2770 (BAY60) inhibits ASM cell migration through phosphorylation of the PKG target and actin-binding VASP. We evaluated the capacity of BAY60 to stimulate cGMP/PKG/pVASP.S239 signaling and assessed its impact on vascular remodeling and ASM cell migration using full-length (FL) VASP overexpressing (wild type, WT) mutants with/without VASP.S239 phospho-mutagenesis. In brief, results show that BAY60 mitigates

vascular remodeling, ASM cell migration and actin dynamics via enhanced cGMP/PKG/VASP yet through mechanisms independent of pVASP.S239.

2. Materials and Methods

Studies outlined in this project abided by the guidelines of the East Carolina University Animal Care and Use Committee and conformed to the Guide for the Care and Use of Laboratory Animals (US National Institutes of Health, Publication No. 85–23, revised 1996).

2.1. Materials

BAY60 was provided as a kind gift from BAYER Pharmaceuticals (Bayer Health Care, Germany). ODQ was purchased from Acros (New Jersey). IBMX was purchased from Calbiochem (Germany). DT2 was purchased from Sigma-Aldrich (Saint Louis, MO). A7r5 (ATCC® CRL1444™) Smooth Muscle Cells were purchased from ATCC (Manassas, VA). Primary antibodies were purchased from Abcam (Cambridge, MA), Cell Signaling (Danvers, MA), or Santa Cruz (Dallas, TX) and secondary antibodies from Rockland (Gilbertsville, Pennsylvania). Phalloidin and DNase 1 were purchased from Invitrogen (Carlsbad, CA). Site-directed mutagenesis system was purchased from Dharmacon (Lafayette, CO).

2.2. Methods

2.3. Cyclic nucleotide content assays—Rat primary ASM cells were seeded in 24-well plates (100,000 cells/well), grown to confluence and analyzed using two different cGMP ELISA kits (Enzo Life Sciences; Farmingdale, NY and Sigma-Aldrich; St. Louis, MO) per manufacturer's instructions and as previously described [32]. Briefly, cells were pretreated with the phosphodiesterase inhibitor IBMX (1 mM) for 15 minutes prior to co-incubation with IBMX with or without the soluble guanylyl cyclase (sGC) inhibitor ODQ (10 μM) containing vehicle (VEH), BAY41-2272 (BAY41; 1 μM) or BAY60 (1 μM) and cGMP content was analyzed after specified times. cGMP estimations were performed after extraction using 0.1 N HCl. The cells were then washed with normal saline and the lysed with 1 N NaOH for protein estimations using the Pierce BCA Protein Assay Kit (Thermo; Waltham, MA) and cyclic nucleotide content was normalized to total protein within each sample.

2.4. Rat carotid artery injury model

Carotid artery (CA) balloon injury was performed as previously described [33–36]. Briefly, male adult (age 6–10 months) Sprague-Dawley rats (Harlan, Indianapolis, IN) were anesthetized using an intraperitoneal injection of ketamine (90mg/ml)/xylazine (10 mg/mL) cocktail (1mL/kg) supplied by the Department of Comparative Medicine, Brody School of Medicine, East Carolina University, Greenville, NC. An arteriotomy of the left external CA was created to allow introduction of a Fogarty 2F embolectomy catheter (Baxter Healthcare Crop., Irvine, CA), which was passed uninflated through the left common CA ending just distal of the aortic arch. The balloon was inflated to 2 atm (0.02 mL) and withdrawn three times to effectively denude the endothelium and cause mural distension of the vessel wall.

The catheter was removed and the external CA ligated to restore blood through the internal and common CA. At this time DMSO (VEH) or BAY60 were mixed in 200 μL Pluronic gel (BASF) and topically administered to the adventitia of the exposed common CA as described [32,35,36]. Animals were closed and allowed to recover before being returned to the animal care facility. Standard rat chow and water was provided through the duration of the study.

2.5. Vascular ultrasound

Vascular ultrasound was performed immediately prior to euthanasia 14 days after balloon injury using the Vevo 2100 High Resolution Imaging System (Visual Sonics Inc., Toronto, Canada) and methods previously described [37]. Hair was depilated (Nair) and a contact gel (Aquasonic, Parker Laboratories, Fairfield, NJ) was applied to the neck to minimize transducer (30 MHz) interference. Identification of the common CA was achieved in B Mode and measurements were recorded in M Mode.

2.6. Tissue processing and staining

Fourteen days after balloon injury and immediately following vascular ultrasound, animals were deeply anesthetized and euthanized by pnuemothorax and exsanguination. In situ perfusion and fixation protocols were performed as described [32,35,36]. Briefly, isotonic saline was perfused transcardially immediately followed by perfusion of 10% formalin buffer in saline. Common CAs were harvested (maintaining appropriate orientation relative to injury and treatment), post-fixed in 10% formalin and stored in 70% ethanol until processing. Vessels were processed in graded alcohols and paraffin-embedded. Five μm sections were cut and mounted on charged slides before deparaffinization and rehydration steps were performed. Verhoeff-Van Gieson staining of elastic tissue was accomplished as described [32,35]. Images were captured microscopically (Leica DM5000B; Leica, Wetzlar, Germany) and analyzed using NIH Image J software.

2.7. Cell culture

Two different ASM cell types were used in this study: rat primary aortic (rat primary) and rat A7r5 aortic (A7r5) ASM cells—For primary cells, male juvenile (age 3–5 months) Sprague-Dawley rats (Harlan, Indianapolis, IN) were deeply anesthetized and euthanized by pnuemothorax and exsanguination. ASM cells were harvested from the thoracic aorta and isolated using mechanical and elastase/collagenase digestion as described [32,35]. Cells were serially passaged in Dulbecco's Modified Eagle Medium supplemented with 10% fetal bovine serum (FBS), and Primocin (100 mg/L; InvivoGen) up to passage 6. Cultures were maintained in sterile conditions with 95% air and 5% CO_2 throughout. Rat A7r5 ASM cells were sub-cultured in identical fashion.

2.8. Migration assays

Two different cell migration assays were used: transwell chemotaxis and scrape wound healing—In both approaches and in consideration of potential confounding effects of cell proliferation, cells were quiesced in low serum (0.2% FBS)-

containing media for 24 hours prior to the initiation of migration assays as previously reported [35].

Transwell chemotaxis assay: As described [35] with minor modifications, ASM cells were stained using CellTracker Green (10 μM; Invitrogen) and seeded on top of Fluoroblok transwell inserts (Corning) and allowed to adhere to the porous membranes (8 μm pores) for 1 hour. Conditioned media and unattached cells were removed from the top insert and replaced with 300 μL of low serum (0.2% FBS) media containing VEH or BAY60 (1, 10, 30 μM). Serum-free media containing platelet derived growth factor (PDGFβ; 10 ng/mL) was added to the bottom reservoirs of each well in order to stimulate unidirectional cell migration. Migration was quantified as a function of fluorescence detected on the bottom of the Fluroblok insert using a bottom read plate reader (Tecan Infinite M200) at 525 nm at different time points over a 20 hour time period.

Scrape wound healing assay: As detailed [32,35] ASM cells were seeded in tissue culture-treated 6 or 12 well plates and grown to confluence. Following quiescence, sterile P200 pipette tips were used to manually create scrape injuries in the center of each well. Excess cellular debris was immediately removed with 1× Dulbecco's phosphate buffered saline (DPBS; Gibco) followed by the addition of complete media containing treatment. Multiple images were captured of each scrape immediately following at times 0 (T0) and 16 hours (T16) post-washout for all non-time lapse experiments using a Leica DMI4000B inverted microscope and CoolSnap HQ2 camera (Photometrics; Tucson, AZ). Migration was expressed as percent recovery by normalizing the average wound width (5 measurements per field) at T16 by the average wound width (5 measurements per field) at T0 per treatment well.

Time lapse imaging: For select wound healing experiments, an automated stage with (X,Y) coordinate control and on-stage incubator were employed (EVOS FL Auto; Life Technologies). Following protocols described above, plates were placed in a humidified chamber maintained at 37°C and 5% CO_2 through the duration of the time-lapse experiment. Beacons were placed in 3 separate locations throughout each scrape injury and images were captured at 15 minute intervals through 16 hours. Using SVCell software (Bellevue, WA), green-colored masks were applied to the wound region and applied to all frames in order to quantify cell recovery normalized to T0 wound area.

2.9. Actin cytoskeletal staining

Globular (G) to filamentous (F) actin ratios were quantified in suspended VEH-and BAY60-treated cells—Following adherent treatment, cells were washed in warm DPBS then trypsinized, clarified through centrifugation and fixed in warm 4% formalin for 10 minutes at 37°C. Fixed cells were clarified again through centrifugation, the fixative was aspirated, and cells were co-stained for 20 minutes at 37°C in phalloidin/DNase1 suspension as previously described with minor modificaitons [35]. G:F actin quantitation was accomplished using the BD FACSVantage flow cytometer (BD Biosciences, San Jose, CA) using 488 nm laser excitation and 515–545 nm emission optics for phalloidin-Alexa Fluor 488 quantiation (F-actin) and 568 nm laser excitation and 619–

641 nm emission optics for DNAseI quantitation (G-actin). At least 5000 cells were analyzed per group using similar morphometric gates. FL-4 signal (G-actin) was divided by FL-1 signal (F-actin) in order to express G:F for each run (normalized to total gated events).

2.10. Kinase activity assays

Treatment was performed in tissue culture-treated plates (6 or 12 well) as described with minor modifications [38]. Cells were lysed in RIPA buffer supplemented with protein phosphatase and protease inhibitor cocktail (1:100; Thermo). Protein was isolated according to manufacturer's instructions and content determined using the Pierce BCA Protein Assay Kit (Thermo). 10 μL of crude lysate was added to each well of a cGMP dependent protein kinase activity kit (CycLex; MBL International Corp.; Woburn, MA). Absorbance was read at 450 nm using a bottom read plate reader (Tecan Infinite M200) and normalized to total protein loaded per well. Full-length and catalytic domain-only recombinant cGMP-dependent protein kinase(s) were used as positive controls.

2.11. Protein detection

Expression of specific proteins was evaluated in ASM cell homogenates and in adherent ASM cells

Protein isolation: Following treatment, cells were washed twice in ice-cold DPBS then lysed using cold RIPA buffer (Thermo) supplemented with Halt protease and phosphatase inhibitor cocktail (Thermo) per manufacturer's instructions. Lysates were gathered and transferred to a centrifuge tube and centrifuged at 14,000×g for 15 minutes at 4°C. Protein content was determined using the Pierce BCA Protein Assay Kit (Thermo).

Enhanced chemiluminescent Western blot: Whole ASM cell lysates were subjected to sodium dodecyl sulfate polyacrylamide gel electrophoresis (SDS-PAGE). Separated protein was transferred to polyvinylidene fluoride (PVDF) membranes with TransBlot Turbo transfer packs (Bio-Rad) using the TransBlot Turbo Transfer System (Bio-Rad) using the high molecular weight setting (10 minutes at 2.5A up to 25V). Membranes were blocked for 1 hour at room temperature in 5% dry milk solution containing 0.1% Tris-buffered saline +Tween-20 (TBST). Following block, membranes were incubated at 4°C in 5% BSA in 0.1% TBST using 1:1000 primary antibodies (unless otherwise noted) with gentle agitation overnight. Membranes were washed in TBST and incubated for 1 hour at room temperature in 5% dry milk+TBST using 1:5000 horseradish peroxidase (HRP) conjugated anti-rabbit secondary antibody (Rockland; Limerick, PA) unless otherwise noted with gentle agitation. Membranes were washed and developed using Super Signal West Pico substrates (Thermo) per manufacturer's instructions. Chemiluminescent signal was detected and analyzed using BioRad's ChemiDocIt imaging system and software.

In-Cell Western assays: Following previously detailed protocols [32,39], ASM cells were seeded in 96-well plates (5,000 cells/well) overnight and treated with VEH or BAY60 (0.1–10 μM) for desired time points. Cells were immunolabeled using rabbit anti-VASP.S239 (1:500; Cell Signaling) or mouse anti α-tubulin (1:500; Sigma) primary antibodies, then labeled using near infrared secondary antibodies (IR680 and IR800; LiCor).

Proteins were quantified by scanning well fluorescence on the IR Odyssey® Imager (CLx, LI-COR Biosciences, Lincoln, NE) and normalized with respect to α-tubulin content.

2.12. Site-directed mutagenesis

The GFP expression vector was purchased from Dharmacon. The pExpress1 expression plasmid containing full-length wild type rat Vasp was used for all VASP transfections (Dharmacon). Site-directed mutagenesis was carried out using the GeneArt Site-Directed Mutagenesis System (Thermo). 5'-CAAACTCAGGAAAG-TGGCCAAGGAGGAGGCCTCT-3' and 5'-AGAGGCCTCCTCCTTGGCCACTTT-CCTGAGTTTG-3' were used as primers to generate a Vasp.S236A mutation (rat homologue of human VASP.S239) and 5'-CAAACTCAGGAAAGTGGACAAGGA-GGAGGCCTCT-3' and 5'-AGAGGCCTCCTCCTTGTCCACTTTCCTGAGTTTG- 3' were used as primers to generate a Vasp.S236D mutation. DNA transformation was carried out using DH5α-T1 competent *E. Coli*. DNA extraction and purification were carried out using the ChargeSwitch-Pro Plasmid Miniprep Kit (Invitrogen) and Qiagen Plasmid Midi Kits (Qiagen). DNA sequencing was confirmed through Eton Bioscience (Research Triangle Park, NC). Transient transfections were performed in complete media on adherent, near confluent cells according to manufacturer's instructions (MBL International Corp.; Woburn, MA). Briefly, 2 μg of DNA was gently mixed with 4 μL Transficient Transfection Reagent (MBL International Corp.; Woburn, MA) in 200 μL of OptiMem (Gibco; Life Technologies). After incubation at room temperature for 10 minutes the DNA-Transficient complex was added to each media charged well (2 mL of complete media per well of a 6 well plate unless otherwise stated) and allowed to transfect for 48 hours.

2.13. qRT-PCR

For transfection verification cells were lysed using TRIzol Reagent and RNA was extracted using Purelink RNA (Invitrogen) according to manufacturer's instructions. RNA levels were quantified using the NanoDrop (Thermo) then 2 μg RNA was reverse transcribed using a high capacity RNA-to-cDNA kit and thermal cycler (BioRad) according to manufacturer's instructions (Life Technologies). Gene expression was quantified using Taqman primers (Life Technologies) and the QuantStudio6 (Life Technologies) using methods previously described [40].

2.14. Transfection efficiency and GFP selection

For select experiments GFP co-transfection was performed by adding 2 μg of GFP containing vector to each FL-VASP group and co-transfected for 48 hours. Following co-transfection cells were trypsinized and subjected to fluorescence activated cell sorting (FACS) using the BD FACSVantage flow cytometer and 488 nm laser excitation and 515–545 nm emission optics for GFP detection. Using naïve (non-transfected/unstained) ASM cells as a baseline, morphologic and autofluorescent gates were established and then two fluorescent regions were designated in order to separate GFP positive from non-GFP containing/negative cells. Cells were sorted directly into lysis buffer and treated as previously described for cell lysates (see section 2.11.). Transfection efficiency was determined as the number of GFP positive cells divided by the total number of viable cells sorted.

2.15. Statistical analysis

Results are presented as mean ± standard error of the mean (SE). Statistical analyses were performed with one-way analysis of variance (ANOVA) followed by Tukey's post-hoc multiple comparison tests for comparisons of three or more groups. Two-way ANOVA was used when two different independent variables impacted one continuous dependent variable. Student's t-test were performed for unpaired groups using Sigma Plot (v11.1). A p-value < 0.05 was considered statistically significant.

3. Results and Discussion

Using rat ASM preparations, key findings from this study show that the heme-independent sGC activator BAY60 reduces arterial remodeling in vivo and ASM cell migration and G:F actin in vitro and stimulates cGMP/PKG/pVASP.S239 signaling. Through use of FL-VASP over-expressing and Ser239-specific, phosphorylation-mimetic and phosphorylation-resistant mutants along with selective pharmacologic blockade, the anti-migratory actions of BAY60 appear to operate primarily via PKG and not through pVASP.S239 as originally anticipated. These results provide evidence that BAY60 through cGMP/PKG has capacity to modulate components of vascular disease pathology and implicate BAY60 as a potential pharmacotherapy against ASM growth disorders such as CAD. Further, we show VASP phosphorylation differentially regulates PKG activity, a novel finding that supports the anti-migratory actions of BAY60 and provides further support for identifying discrete PKG-mediated mechanisms capable of inhibiting ASM cell migration in the context of CAD.

3.1. BAY60 potentiates cGMP content following sGC oxidation

Pankey and colleagues [41] recently showed that BAY60 possesses vasodilator activity in rat pulmonary and systemic vasculature by increasing catalytic activity of heme-oxidized sGC in vivo. However, the impact of BAY60 on ASM cell culture has not yet been described. In turn, we examined mechanisms elicited by BAY60 as well as the heme-dependent sGC stimulator BAY 41-2272 (BAY41) in rat primary ASM cells. Using a cGMP-specific competitive ELISA, both BAY41 and BAY60 significantly increased cGMP levels compared to VEH controls; however, in the presence of the heme oxidant ODQ [42], the BAY41-mediated cGMP increase was fully reversed while the stimulatory effect of BAY60 on cGMP was significantly potentiated compared to BAY60 without ODQ (Figure 1A). Our results are complementary to a recent study [5] whereby BAY60 significantly and dose-dependently increased cGMP content which was potentiated with concomitant ODQ in human platelets. To investigate its kinetics, BAY60 (0.001–10 μM) significantly increased cGMP content in concentration- and time-dependent fashion (Figures 1B, C), with peak content achieved using 1 μM BAY60 after 15 minutes with sustained elevation through 2 hours. In parallel experiments BAY60 (0.001–10 μM) did not significantly alter cAMP levels (data not shown). These results demonstrate ability of BAY60 to selectively increase cGMP production via heme-independent sGC activation yet without marked effects on cAMP signaling.

3.2. BAY60 reduces arterial remodeling in vivo

BAY60 has been previously used to produce pulmonary and systemic vasodilation independent of endogenous nitric oxide or reduced heme (43), but to our knowledge BAY60 has not yet been characterized as a mediator of vascular remodeling following balloon angioplasty, a primary endovascular intervention performed in human coronary arteries [1]. The rat carotid artery balloon injury model is well-established for evaluating ASM growth under in vivo conditions [43,44]; therefore, we used this model to investigate the ability of BAY60 to mitigate or prevent arterial growth and remodeling. Perivascular application of BAY60 immediately after injury significantly reduced neointimal formation and significantly increased lumen diameter compared to VEH controls after 14 days (Figure 2A–D). Representative photomicrographs of Verhoff-van Gieson-stained arterial cross-sections 14 days post-injury are shown for an injured, VEH-treated vessel (Figure 2A) and for an injured, BAY60-treated vessel (Figure 2B). In parallel, and to consider potential limitations associated with histomorphometry such as tissue shrinkage and/or distortion of cellular components, non-invasive vascular ultrasound was performed prior to euthanasia 14 days after injury. In agreement with histological findings, quantitation of vascular sonograms revealed BAY60 significantly increased lumen diameter compared to VEH controls (Figure 2E–G). Representative tracings from in vivo vascular ultrasound for VEH (Figure 2E) and BAY60-treated (Figure 2F) carotid arteries are shown. The importance of in vivo sGC signaling following carotid injury was highlighted by Sinnaeve and colleagues [45,46] where they found sGC subunit gene transfer and overexpression of constitutively active PKG reduced neointima formation following rat balloon injury. Conflicting findings were observed by Wolfsgruber et al. [47] who showed a proatherogenic role of PKG in mouse ASM cells. Due to the difference in species and experimental models between these two studies it is difficult to ascertain the specific mechanism(s) through which smooth muscle growth is modulated. There are a number of studies which show opposing actions of NO and cGMP in modulating arterial remodeling; please see [16] for a good review on this topic. We have previously shown using distinct pharmacologic heme-dependent sGC stimulators such as BAY41 [32] or YC-1 [48] that reduced arterial remodeling following mechanical injury was possible through enhanced cGMP signaling. Importantly, the use of the heme-independent sGC activator BAY60 to moderate injury-induced in vivo ASM growth has not been reported until now.

3.3. BAY60 inhibits ASM cell migration in vitro

Considering that cellular migration is a key component of arterial remodeling, we next evaluated the impact of BAY60 on migration using rat ASM cells and two distinct in vitro migration assays. With a serum-stimulated wound healing assay and rat primary ASM cells, BAY60 (30 μM) significantly reduced random cell migration (chemokinesis) and wound recovery after 16 hours compared to VEH controls (Figure 3A). Because ASM cell motility in vascular pathology involves not only chemokinesis but also directed translocation down a concentration gradient (chemotaxis) [49], we utilized a transwell apparatus and PDGFβ-stimulation to measure this chemotactic response. BAY60 significantly and dose-dependently (1–30 μM) reduced rat primary cell migration compared to VEH controls over 20 hours (Figure 3B). These findings demonstrate ability of BAY60 to inhibit random as well as directed migration in rat primary ASM cells. In order to replicate these findings in

other ASM cell types we examined the anti-migratory effects of BAY60 on rat A7r5 ASM cells. Using a traditional wound healing assay paired with an on-stage incubator equipped with automated stage and (X,Y) coordinate controls along with a newly developed, highly sensitive wound healing analysis program (SVCell; Bellevue, WA), BAY (10 μM) significantly reduced A7r5 ASM cell migration versus VEH controls over 16 hours (Figures 3C–G). Photomicrographs of green-masked confluent cells treated with VEH or BAY60 immediately after wounding (time 0; Figures 3C, E, resp.) or 16 hours after wounding (time 16hr; Figures 3D, F, resp.), along with automated quantitation through 16 hours are shown (Figure 3G). These cumulative cell migration findings using BAY60 are consistent with results obtained using different sGC stimulators which were previously shown to prevent ASM chemokinesis and chemotaxis [32,50].

3.4. BAY60 decreases G:F actin

ASM cells, like many other adherent cell types, rely on reorganization of their actin cytoskeleton as a primary mechanism for movement [51]. Therefore, to assess the capacity of BAY60 to control actin cytoskeletal dynamics central to cell migration, two separate approaches were used in rat primary and A7r5 ASM cells. Following VEH or BAY60 treatment cells were trypsinized, fixed, stained and subjected to flow cytometry in order to quantify G:F actin. Representative scatter plots and histograms for unstained, VEH- or BAY60-treated cells for both F- and G-actin are shown (Figures 4A–C). Using this approach, an 80% reduction in G:F was evident in BAY60-treated rat primary cells compared to VEH controls while a statistically significant reduction in BAY60-treated A7r5 cells was also observed after 1 hour (Figure 4D). Together, these data suggest BAY60 promotes F actin formation after 1 hour which remains elevated through 16 hours. Although analysis of G:F actin is an accepted approach for predicting the migratory status of adherent cells at a given point in time [52], measuring G:F actin cannot stand alone in the absence of a functional measurement of cellular migration (as described above) in light of numerous reports providing sound evidence for bi-directional movement of G:F actin in the context of migration [23,35,52,53].

3.5. BAY60 increases PKG activity and VASP S239 phosphorylation

Because cGMP traditionally binds to the regulatory subunit of PKG effectively releasing its active catalytic subunit we sought to determine if BAY60 could stimulate PKG activity subsequent to cGMP induction. BAY60 (10 μM) significantly increased PKG activity compared to VEH controls in rat primary and A7r5 ASM cells after 60 mins (Figure 5A). These data show that BAY60 operates in canonical cGMP/PKG fashion in rat ASM cells. We then evaluated pVASP.S239 expression, a primary phosphorylation target of PKG [26], in both ASM cell types. Following 1 hour of BAY60 (10 μM) treatment, whole cell homogenates using ECL Western blotting techniques for pVASP.S239 expression, showed pVASP.S239 expression significantly increased compared to VEH controls (Figure 5B) with a representative blot shown in Figure 5C. InCell Western blotting on intact, adherent rat primary ASM cells demonstrated similar results (Figure 5D). Considering promiscuity for cyclic nucleotide-directed kinase signals, the preferred PKA target VASP-Serine157 (VASP.S157) was also probed, and results showed that BAY60 also significantly increased pVASP.S157 expression but not to the same degree as pVASP.S239 (data not shown). In line

with our recently published findings in rat primary ASM cells using the heme-dependent sGC stimulator BAY41 [32], we speculate that the increase in pVASP.S157 occurred secondary to BAY60-induced cGMP/PKG/ pVASP.S239 signaling via kinase crosstalk. An elegant study by Butt and colleagues [30] further supports this finding where they showed PKG preferentially phosphorylates VASP on Ser239, but also phosphorylates VASP on Ser157 with similar kinetics.

3.6. VASP-specific site-directed mutagenesis

The actin-binding protein VASP can modulate F-actin polymerization at the leading edge of migrating cells [25,51,54] and VASP phosphorylation has been postulated not only as a readout for PKG activity but also as a means for modulating its function [23,24]. Consistent with the observations that BAY60 increased cGMP/PKG and particularly pVASP.S239 and also reduced ASM cell migration, we theorized that the anti-migratory capacity of BAY60 is pVASP.S239-dependent. In order to test this hypothesis we performed site-directed mutagenesis (SDM) to transiently overexpress full length wild type VASP (FL-VASP/WT) with/without Ser239 phosphorylation-mimetic (FL-VASP/ 239D) and phosphorylation-resistant (FL-VASP/239A) mutations. SDM is a well characterized method for replacing targeted amino acid residues with uncharged (Alanine-A) or negatively charged (Aspartate-D) amino acids in order to mimic a constitutively phosphorylated (D) or a dominant negative/non-phosphorylated (A) resistant mutant [23].

All of the transient transfections and SDM analyses were performed using wild type A7r5 ASM cells that possess endogenous VASP to more fully replicate the normal condition. Commercial rat A7r5 ASM cells (ATCC) are characterized as primary thoracic aorta-derived cells, yet we and others appreciate the phenotypic differences that can sometimes exist between primary and commercial cells [55–57]. Nonetheless, for the cell signaling and functional endpoints examined in this study and others recently published by our lab [57,58], strikingly similar responses were observed following pharmacologic treatment for rat primary and A7r5 ASM cells; in turn, for the VASP mutant studies A7r5 ASM cells were used. Of note, to our knowledge we are the first group to conduct transient overexpression studies using an A7r5 WT background. Most VASP overexpression or mutagenesis studies have used aortic ASM cells harvested from $VASP^{-/-}$ mice and retroviral constructs encoding mutant human VASP [31,59]. However, in addition to performing experiments in $VASP^{-/-}$ ASM cells Chen et al. [31] additionally showed effects of VASP transfection into Fisher 344 rats already containing VASP using a Tetracycline-Inducible System, but these studies evaluated cell proliferation and not migration.

In designing our experiments we were reluctant to incorporate a selection marker for assessment of plasmid expression due to the potential negative impact that a large differentiation marker could have on normal VASP function [60]. Therefore, in order to verify transfection efficiency, initial experiments were performed using a co-transfection model [61] consisting of a GFP-containing vector in the presence or absence of FL-VASP vectors which were co-transfected for 48 hours so that GFP expression serves as a function of SDM transfection efficiency at this time point. Photomicrographs of naïve and transfected groups under phase at time 0 (T0) and after 48 hours as well as fluorescent images for GFP

expression at 48 hours are shown in Figure 6A. We also quantitatively validated transfection efficiency using percent GFP-positive cells (Figure 6B) which showed consistently around 50% transfection efficiency across treatment groups without impacting cell viability (data not shown). Furthermore, transcript analysis via qRT-PCR and protein analysis by Western blotting were performed in naïve/non-transfected cells, FL-VASP/WT, FL-VASP/239D and FL-VASP/239A over-expressing cells. Results show that each of the FL-VASP transfected cells transiently overexpress over 4000-fold the transcript levels for total VASP compared to naïve control cells (normalized to GAPDH) (data not shown) and 3 times the level of total VASP protein compared to naïve, transfection vehicle, and vector-only control cells 48 hours post-transfection (Figures 6C–D). Western blotting for total VASP protein showed a distinct and intense protein band just above 50kD in all FL-VASP transfected groups which was not apparent in any of the other control groups (Figure 6C–D). Because DNA sequences were confirmed for rat FL-VASP prior to carrying out these experiments and considering a potential influence of translational read-through we are confident that this large protein is transfected exogenous VASP. To further verify our transfection efficiencies and to show that this heavier molecular weight (MW) protein was not simply an artifact of transfection we performed FACS to separate (from the same transfected flask) all of the GFP positive from GFP negative cells (experimental scheme for FACS cell sorting is shown in Figure 6E). It is clear in Figure 6F that the heavier MW band is only present in the GFP/FL-VASP/WT positive cell lysate and is not evident in the GFP negative cells sorted from the same flask. In all, these findings validate our SDM methodology and approach for transfecting and significantly modulating VASP expression in A7r5 ASM cells.

3.7. Biological activities of FL-VASP mutants and the influence of BAY60

In order to evaluate the FL-VASP mutant phenotypes and to test the effects of BAY60 on ASM cell endpoints, the same conditions used for BAY60 treatment of naïve A7r5 ASM cells as described above were employed. Migration, PKG and PKA activities were assessed in VEH and BAY60-treated overexpressing FL-VASP/ WT, FL-VASP/239D, and FL-VASP/ 239A mutants. We anticipated that supplementing endogenous VASP with transient overexpression of exogenous rat FL-VASP/WT would inhibit ASM cell migration, possibly by providing more substrate for PKG-mediated events to occur. We also expected our phosphorylation-mimetic, constitutively active FL-VASP/239D group would show significantly inhibited cell migration since this overexpression would most closely resemble our previously characterized anti-migratory phenotype and VASP induction observed with BAY60 treatment (see Figures 3, 5). Conversely, we expected to see a reversal of these effects or an increase in migration compared to naïve cells when we overexpressed phosphorylation-resistant FL-VASP/239A due to the rationale that inhibition of migration would be pVASP.S239-dependent. Though independently, we expected all three untreated FL-VASP groups to demonstrate different migratory phenotypes, we did not expect to see a significant change in these migratory phenotypes when treated with BAY60. This was theorized because our observational results led us to believe BAY60 operated to inhibit ASM cell migration in pVASP.S239-dependent fashion.

Interestingly, when using the scrape injury to assess cell migration, the FL-VASP/WT (total VASP overexpressing) and phospho-resistant FL-VASP/239A groups showed significantly

reduced migration after 16 hours yet this was negated with phospho-mimetic FL-VASP/239D overexpression (Figures 7A–B). Although we expected FL-VASP/WT to inhibit migration, in support of a study using cultured rat fibroblasts (Rat2 cell line) showing FL-VASP/WT overexpression attenuated cell migration through defining or maintaining cell polarity [54], our findings using FL-VASP/239A overexpressing ASM cells was not anticipated. However, Defawe and colleagues [59] performed ASM cell invasion assays using mouse $VASP^{-/-}$ cells and showed that FL-VASP/239D enhanced migration compared to phosphorylation-resistant FL-VASP/239A mutants, but the differences in experimental design to include comparisons to a naïve untreated group prevent direct comparisons of results.

Scrape injuries were then performed in the VASP mutants in the absence or presence of BAY60. BAY60 did not significantly impact FL-VASP/WT or FL-VASP/239A mutant ASM cell migration 16 hours post-injury when compared to corresponding VEH-treated groups; however, FL-VASP/239D overexpression in the presence of BAY60 significantly reduced migration compared to its VEH control (Figure 7C). Because BAY60 significantly increased PKG activity (see Figure 5A), we theorized that perhaps pVASP.S239 modulates upstream PKG activity which in turn could regulate ASM cell migration independent of VASP phosphorylation status. This idea had not been cited in the literature to date although others have evaluated alternate kinases impacted by VASP phosphorylation [59]. In turn, we analyzed the influence of the VASP mutants on PKG activity. FL-VASP/WT significantly elevated PKG activity compared to naïve cells (Figure 8A). Further, and in support of our anti-migratory findings with BAY60, FL-VASP/239D abrogated the stimulatory effects of FL-VASP/WT and FL-VASP/239A on PKG activity (Figure 8B). To address potential changes that might occur in other predominantly cited kinases that phosphorylate VASP we also evaluated PKA activity using a similar ELISA as described for measuring PKG activity. We found that none of the VASP mutants significantly altered PKA activity compared to naïve cells (Figure 8C). To extend and confirm our suspicion that FL-VASP/WT overexpression modulates PKG activity and is not merely a byproduct of transfection, following co-transfection FACS sorting (following the schematic shown in Figure 6E) was performed, and results show that only the GFP-containing FL-VASP/WT cells showed significantly increased PKG activity compared to GFP-negative cells from the same flask (Figure 8D). This differential regulation of PKG activity by VASP could possibly explain the significant reduction in ASM cell migration only seen in the FL-VASP/239D group (Figure 7C). This finding might also explain the inability of BAY60 to affect ASM cell migration in FL-VASP/WT and FL-VASP/239A overexpressing ASM cells due to a PKG saturation effect.

3.8. PKG blockade reverses BAY60-induced attenuation of ASM cell migration

As the anti-migratory effects of BAY60 seem to be independent of pVASP.S239 based on these findings, we tested the role of PKG in modulating BAY60-induced inhibition of ASM migration in non-transfected cells. Using the well-characterized PKG inhibitor DT-2 that we and others have validated for PKG blockade in ASM cells [32,62,63], results show that PKG inhibition fully reversed BAY60-induced reduction of ASM cell migration (Figure 9). Negash and colleagues [64] suggested that PKG mediates pulmonary ASM cell migration

using a similar pharmacologic inhibitor, but these effects were determined to be hypoxiadependent. Our data provide evidence that BAY60 inhibits migration of ASM cells through mechanisms reliant at least in part upon active PKG. We believe that phosphorylated VASP.S239 could also be a consequence of elevated PKG signaling yet appears not to be involved as a regulatory mechanism for BAY-mediated reduction in cell migration.

3.9. Clinical relevance of BAY60

Brief discussion is warranted for the potential clinical importance for BAY60 in combating vascular proliferative disorders. From early efforts to develop pharmacologic approaches to enhance cGMP signaling, two broad classes of compounds were developed: heme-dependent sGC stimulators and heme-independent sGC activators [65]. Previous studies in our lab have shown molecular, cellular, and functional mechanisms of heme-dependent sGC stimulators such as YC-1 and BAY 41-2272 in ASM under in vivo and in vitro conditions [32,34,59,66]. While heme-dependent sGC stimulators require an operational/reduced sGC heme moiety in order to function, heme-independent activators such as BAY60 have capacity to operate in heme-deficient or heme-oxidized tissues, conditions often found during cardiovascular disorders [67] and a capacity validated in initial efforts in this study (see Figure 1A) The effects of BAY60 in ASM are therapeutically intriguing yet heretofore have been undefined and thus were the focus of the current study. To date, sparse scientific evidence exists regarding the influence of BAY60 on ASM pathologic growth. Some earlier studies with BAY60 showed attenuation of liver fibrosis in a rat model, suggestive of a therapeutic approach for liver fibrosis [68], and an inhibitory effect on platelet aggregation, adhesion and intracellular Ca^{2+} levels in human platelets under oxidized conditions [5]. Other reports have shown that systemic BAY60 has capacity to decrease pulmonary arterial pressure and systemic arterial pressure in a rat model, suggesting a regulatory role for BAY60 on vasodilation of pulmonary and systemic vasculature [41]. BAY60 has also been identified to preserve sGC activation and cGMP signaling in the oxidative conditions of cardiac stress [69]. While these studies suggest promising therapeutic roles for BAY60, similar sGC activators (Cinaciguat or BAY 58-2667) have been discontinued in clinical trials due to off-target hypotensive effects [22]. However, use of these compounds delivered locally and aimed at ameliorating adverse vascular remodeling and/or intervention-induced restenosis has not been tested. In light of the results presented in this study we demonstrate clinically appealing ability of BAY60 to control aspects of aberrant ASM growth and pose that if delivered locally may prevent the adverse outcomes experienced during clinical trials.

4. Conclusions

Findings from this study show that BAY60 can reduce pathologic ASM growth under in vivo and in vitro conditions possibly through modulation of actin cytoskeleton and via cGMP/PKG/VASP signaling. We also demonstrate that VASP phosphorylation differentially regulates PKG activity, a novel finding that supports the anti-migratory actions of BAY60 and argues pVASP.S239 is involved yet not responsible for the anti-migratory actions of BAY60. Taken together, these findings implicate that BAY60 has therapeutic capacity as a growth regulator in ASM and may provide an approach to moderate vascular growth disorders.

Acknowledgments

The authors would like to thank Drs. J. P. Stasch and A. Knorr (Bayer HealthCare AG, Berlin, Germany) for the generous gift of BAY 60-2770, Dr. Bill Angus (Dept. of Biochemistry) for his help with the site-directed mutagenesis studies, and Dr. Joe McClung (Dept. of Physiology), for his assistance in performing time-lapse migration experiments.

Grants This project was supported by the Chapter 33 Post 9/11 GI Bill (AWH), by Award Number R01HL081720 from the National Institutes of Health National Heart, Lung, and Blood Institute (NHLBI) (DAT), ARRA Award Number R01HL081720-03S2 (DAT), NHLBI Post-doctoral Research Supplement Award Number R01HL081720-05S1 (DAT), an ECU Brody School of Medicine Seed/Bridge Grant (DAT), and a Brody Brothers Endowment Fund Award (DAT). The content is solely the responsibility of the authors and does not necessarily represent the official views of the National Heart, Lung, and Blood Institute, the National Institutes of Health, or the Brody Brothers Endowment Fund.

References

1. Mozaffarian D, Benjamin EJ, Go AS, Arnett DK, Blaha MJ, Cushman M, Das SR, Ferranti S, Després JP, Fullerton HJ, Howard VJ, Huffman MD, Isasi CR, Jiménez MC, Judd SE, Kissela BM, Lichtman JH, Lisabeth LD, Liu S, Mackey RH, Magid DJ, McGuire DK, Mohler ER, Moy CS, Muntner P, Mussolino ME, Nasir K, Neumar RW, Nichol G, Palaniappan L, Pandey DK, Reeves MJ, Rodriguez CJ, Rosamond W, Sorlie PD, Stein J, Towfighi A, Turan TN, Virani SS, Woo D, Yeh RW, Turner MB. AHA Statistical Update: Heart Disease and Stroke Statistics 2016 Update: A Report From the American Heart Association. Circulation. 2015 published online before print December 16, 2015.
2. Buys ES, Raher MJ, Kirby A, Mohd S, Baron DM, Hayton SR, Tainsh LT, Sips PY, Rauwerdink KM, Yan Q, Tainsh RE, Shakartzi HR, Stevens C, Decaluwe K, Rodrigues-Machado MG, Malhotra R, Van de Voorde J, Wang T, Brouckaert P, Daly MJ, Bloch KD. Genetic modifiers of hypertension in soluble guanylate cyclase alpha1-deficient mice. J Clin Invest. 2012; 122:2316–2325. [PubMed: 22565307]
3. Chen L, Daum G, Fischer JW, Hawkins S, Bochaton-Piallat ML, Gabbiani G, Clowes AW. Loss of expression of the beta subunit of soluble guanylyl cyclase prevents nitric oxide-mediated inhibition of DNA synthesis in smooth muscle cells of old rats. Circ Res. 2000; 86:520–525. [PubMed: 10720413]
4. Ross R, Glomset JA. Atherosclerosis and the arterial smooth muscle cell. Science. 1973; 180:1332–1339. [PubMed: 4350926]
5. Mendes-Silverio CB, Leiria LOS, Morganti RP, Anhe GF, Marcondes S, Monica FZ, De Nucci G, Antunes E. Activation of haem-oxidized soluble guanylyl cyclase with BAY 60–2770 in human platelets lead to overstimulation of the cyclic GMP signaling pathway. PLoS One. 2012; 7:e47223. First published November 8, 2012. [PubMed: 23144808]
6. Stasch JP, Hobbs AJ. NO-independent, haem-dependent soluble guanylate cyclase stimulators. Handb Exp Pharmacol. 2009; 191:277–308. 2009. [PubMed: 19089334]
7. Bauters C, Isner JM. The biology of restenosis. Prog Cardiovasc Dis. 1997; 40:107–116. [PubMed: 9327827]
8. Andrew PJ, Mayer B. Enzymatic function of nitric oxide synthases. Cardiovasc Res. 1999; 43:521–531. [PubMed: 10690324]
9. Kubes P, Suzuki M, Granger DN. Nitric oxide: an endogenous modulator of leukocyte adhesion. Proc Natl Acad Sci. 1991; 88:4651–4655. [PubMed: 1675786]
10. Palmer RMJ, Ferige AG, Moncada S. Nitric oxide release accounts for the biological activity of endothelium-derived relaxing factor. Nature. 1987; 327:524–526. [PubMed: 3495737]
11. Radomski MW, Palmer RMJ, Moncada S. Modulation of platelet aggregation by an L-arginine-nitric oxide pathway. Trends Pharmacol Sci. 1991; 12:87–88. [PubMed: 1647064]
12. Scott-Burden T, Vanhoutte PM. The endothelium as a regulator of vascular smooth muscle proliferation. Circulation. 1993; 87:V51–V55.

13. Brophy CM, Woodrum DA, Pollock J, Dickinson M, Komalavilas P, Cornwell TL, Lincoln TM. cGMP-dependent protein kinase expression restores contractile function in cultured vascular smooth muscle cells. J Vasc Res. 2002; 39:95–103. [PubMed: 12011581]

14. Fan GC, Kranias EG. Small heat shock protein 20 (HspB6) in cardiac hypertrophy and failure. J Mol Cell Cardiol. 2011; 51:574–577. First published September 30, 2010. [PubMed: 20869365]

15. McLemore EC, Tessier DJ, Thresher J, Komalavilas P, Brophy CM. Role of the small heat shock proteins in regulating vascular smooth muscle tone. JACS. 2005; 201:30–36.

16. Feil R, Lohmann SM, de Jonge H, Walter U, Hofmann F. Cyclic GMP-dependent protein kinases and the cardiovascular system insights from genetically modified mice. Circulation Research. 2003 Nov 14; 93(10):907–916. [PubMed: 14615494]

17. Woodrum D, Pipkin W, Tessier D, Komalavilas P, Brophy CM. Phosphorylation of the heat shock-related protein, HSP20, mediates cyclic nucleotide-dependent relaxation. J Vasc Surg. 2003; 37:874–881. [PubMed: 12663991]

18. Aggarwal S, Gross CM, Rafikov R, Kumar S, Fineman JR, Ludewig B, Jonigk D, Black SM. Nitration of tyrosine 247 inhibits protein kinase G-1α activity by attenuating cyclic guanosine monophosphate binding. J Biol Chem. 289:7948–7961. First published January 27, 2014. [PubMed: 24469460]

19. Dey NB, Lincoln TM. Possible involvement of Cyclic-GMP-dependent protein kinase on matrix metalloproteinase-2 expression in rat aortic smooth muscle cells. Mol Cell Biochem. 2012; 368:27–35. First published May 23, 2012. [PubMed: 22618526]

20. Li SJ, Sun NL. Regulation of intracellular Ca2+ and calcineurin by NO/PKG in proliferation of vascular smooth muscle cells. Acta Pharmacol Sin. 2005; 26:323–328. [PubMed: 15715928]

21. Yang HM, Kim BK, Kim JY, Kwon YW, Jin S, Lee JE, Cho HJ, Lee HY, Kang HJ, Oh BH, Park YB, Kim HS. PPARγ modulates vascular smooth muscle cell phenotype via a protein kinase G-dependent pathway and reduces neointimal hyperplasia after vascular injury. Exp Mol Med. 2013; 45:e65. [PubMed: 24287871]

22. Erdmann E, Semigran MJ, Nieminen MS, Gheorghiade M, Agrawal R, Mitrovic V, Mebazaa A. Cinaciguat, a soluble guanylate cyclase activator, unloads the heart but also causes hypotension in acute decompensated heart failure. Eur Heart J. 2013; 34(1):57–67. [PubMed: 22778174]

23. Doppler HR, Bastea LI, Lewis-Tuffin LJ, Anastasiadis PZ, Storz P. Protein kinase D1-mediated phosphorylations regulate vasodilator-stimulated phosphoprotein (VASP) localization and cell migration. J Biol Chem. 2013; 288:24382–24393. First published July 11, 2013. [PubMed: 23846685]

24. Thomson DM, Ascione MP, Grange J, Nelson C, Hansen MD. Phosphorylation of VASP by AMPK alters actin binding and occurs at a novel site. Biochem Biophys Res Commun. 2011; 414:215–219. First published September 17, 2011. [PubMed: 21945940]

25. Trichet L, Sykes C, Plastino J. Relaxing the actin cytoskeleton for adhesion and movement with Ena/VASP. J Cell Biol. 2008; 181:19–25. First published March 31, 2008. [PubMed: 18378777]

26. Waldmann R, Nieberding M, Walter U. Vasodilator-stimulated protein phosphorylation in platelets is mediated by cAMP-and cGMP-dependent protein kinases. Eur J Biochem. 1987; 167:441–448. [PubMed: 2820726]

27. Cheng AM, Rizzo-DeLeon N, Wilson CL, Lee WJ, Tateya S, Clowes AW, Schwartz MW, Kim F. Vasodilator-stimulated phosphoprotein protects against vascular inflammation and insulin resistance. Am J Physiol Endocrinol Metab. 2014; 307:E571–E579. First published August 12, 2014. [PubMed: 25117404]

28. Henes J, Schmit MA, Morote-Garcia JC, Mirakaj V, Kohler D, Glover L, Walter U, Karthausen Jm, Colgan SP, Rosenberger P. Inflammation-associated repression of vasodilator-stimulated phosphoprotein (VASP) reduces alveolar-capillary barrier function during acute lung injury. FASEB J. 2009; 23:4244–4255. First published August 18, 2009. [PubMed: 19690214]

29. Aizawa T, Wei H, Maino JM, Abe J, Berk BC, Yan C. Role of phosphodiesterase 3 in NO/cGMP-mediated antiinflammatory effects in vascular smooth muscle cells. Circ Res. 2003; 93:406–413. [PubMed: 12919948]

30. Butt E, Abel K, Krieger M, Palm D, Hoppe V, Hoppe J, Walter U. cAMP- and cGMP-dependent protein kinase phosphorylation sites of the focal adhesion vasodilator-stimulated phosphoprotein

(VASP) in vitro and in intact human platelets. J Biol Chem. 1994; 269:14509–14517. [PubMed: 8182057]

31. Chen L, Daum G, Chitaley K, Coats SA, Bowen-Pope DF, Eigenthaler M, Thumati NR, Walter U, Clowes AW. Vasodilator-stimulated phosphoprotein regulates proliferation and growth inhibition by nitric oxide in vascular smooth muscle cells. Arterioscler Thromb Vasc Biol. 2004; 24:1403–1408. [PubMed: 15178555]
32. Joshi CN, Martin DN, Fox JC, Mendelev NN, Brown TA, Tulis DA. The soluble guanylate cyclase stimulator BAY 41–2272 inhibits vascular smooth muscle growth through the cAMP-dependent protein kinase and cGMP-dependent protein kinase pathways. J Pharmacol Exp Thera. 2011; 339:394–402. First published August 8, 2011.
33. Holt AW, Tulis DA. Experimental Rat and Mouse Carotid Artery Surgery: Injury & Remodeling Studies. ISRN Minim Invasive Surg. 2013 Article ID 167407, 10 pages.
34. Keswani AN, Peyton KJ, Durante W, Schafer AI, Tulis DA. The cyclic GMP modulators YC-1 and zaprinast reduce vessel remodeling through anti-proliferative and pro-apoptotic effects. J Cardiovasc Pharmacol Ther. 14:116–124. First published April 2, 2009. [PubMed: 19342499]
35. Stone JD, Narine A, Shaver PR, Fox JC, Vuncannon JR, Tulis DA. AMP-activated protein kinase inhibits vascular smooth muscle cell proliferation and migration and vascular remodeling following injury. Am J Physiol Heart Circ Physiol. 2013; 304:H369–H381. First published November 30, 2012. [PubMed: 23203966]
36. Tulis DA. Histological and morphometric analyses for rat carotid balloon injury model. Methods Mol Med. 2007; 139:31–66. [PubMed: 18287663]
37. Johnson TL, Tulis DA, Keeler BE, Virag JA, Lust RM, Clemens S. The dopamine D3 receptor knockout mouse mimics aging-related changes in autonomic function and cardiac fibrosis. PloS One. 2013; 8:e74116. First published August 30, 2013. [PubMed: 24023697]
38. Adderley, SP.; Joshi, CN.; Martin, DN.; Mooney, S.; Tulis, DA. Multiple Kinase Involvement in the Regulation of Vascular Growth. In: Da Silva Zavier, G., editor. Advances in Protein Kinases. Vol. Chapter 6. 2012. p. 131-150.InTech Open Access Publishers ISBN 978-953-51-0633-3
39. Chen H, Kovar J, Sissons S, Cox K, Matter W, Chadwell F, Luan P, Vlahos CJ, Schutz-Geschwender A, Olive DM. A cell-based immunocytochemical assay for monitoring kinase signaling pathways and drug efficacy. Anal Biochem. 2005; 338:136–142. [PubMed: 15707944]
40. Zamilpa R, Ibarra J, de Castro Brás LE, Ramirez TA, Nguyen N, Halade GV, Zhang J, Dai Q, Dayah T, Chiao YA, Lowell W, Ahuja SS, D'Armiento J, Jin YF, Lindsey ML. Transgenic overexpression of matrix metalloproteinase-9 in macrophages attenuates the inflammatory response and improves left ventricular function post-myocardial infarction. J Mol Cell Cardiol. 2012; 53:599–608. First published August 3, 2012. [PubMed: 22884843]
41. Pankey EA, Bhartiya M, Badejo AM Jr, Haider U, Stasch JP, Murthy SN, Nossaman BD, Kadowitz PJ. Pulmonary and systemic vasodilator responses to the soluble guanylyl cyclase activator, BAY 60–2770, are not dependent on endogenous nitric oxide or reduced heme. Am J Physiol Heart Circ Physiol. 2011; 300:H792–H802. First Published January 7, 2011. [PubMed: 21217076]
42. Zhao Y, Brandish PE, DiValentin M, Schelvis JP, Babcock GT, Marletta MA. Inhibition of soluble guanylate cyclase by ODQ. Biochemistry. 2000 Sep 5; 39(35):10848–10854. [PubMed: 10978171]
43. Clowes AW, Reidy MA, Clowes MM. Mechanisms of stenosis after arterial injury. Lab Invest. 1983; 49:208–215. [PubMed: 6876748]
44. Tulis DA. Rat carotid artery balloon injury model. Methods Mol Med. 2007; 139:1–30. [PubMed: 18287662]
45. Sinnaeve P, Chiche J, Nong Z, Varenne O, Van Pelt N, Gillijns H, Janssens S. Soluble guanylate cyclase $\alpha 1$ and $\beta 1$ gene transfer increases NO responsiveness and reduces neointima formation after balloon injury in rats via antiproliferative and antimigratory effects. Circulation. 2001; 88:103–109.
46. Sinnaeve P, Chiche J, Gillijns H, Van Pelt N, Wirthlin D, Van de Werf F, Janssens S. Overexpression of a constitutively active protein kinase G mutant reduces neointima formation and in-stent restenosis. Circulation. 2002; 105:2911–2916. [PubMed: 12070122]

47. Wolfsgruber W, Feil S, Brummer S, Kuppinger O, Hofmann F, Feil R. A proatherogenic role for cGMP-dependent protein kinase in vascular smooth muscle cells. Proceedings of the National Academy of Sciences. 2003 Nov 11; 100(23):13519–13524.
48. Tulis DA, Durante W, Peyton KJ, Chapman GB, Evans AJ, Schafer AI. YC-1, a benzyl indazole derivative, stimulates vascular cGMP and inhibits neointima formation. Biochem Biophys Res Commun. 2000; 279:646–652. [PubMed: 11118339]
49. Louis SF, Zahradka P. Vascular smooth muscle cell motility: From migration to invasion. Exp Clin Cardiol. 2010; 15:e75–e85. [PubMed: 21264073]
50. Tulis DA, Bohl Masters KS, Lipke EA, Schiesser RL, Evans AJ, Peyton KJ, Durante W, West JL, Schafer AI. YC-1-mediated vascular protection through inhibition of smooth muscle cell proliferation and platelet function. Biochem Biophys Res Commun. 2002; 291:1014–1021. [PubMed: 11866467]
51. Reinhard M, Jouvenal K, Tripier D, Walter U. Identification, purification, and characterization of a zyxin-related protein that binds the focal adhesion and microfilament protein VASP (vasodilator-stimulated phosphoprotein). Proc Natl Acad Sci. 1995; 92:7956–7960. [PubMed: 7644520]
52. Cramer LP, Briggs LJ, Dawe HR. Use of fluorescently labelled deoxyribonuclease I to spatially measure G-actin levels in migrating and non-migrating cells. Cell Motil Cytoskeleton. 2002; 51:27–38. [PubMed: 11810694]
53. Blume C, Benz PM, Walter U, Ha J, Kemp BE, Renne T. AMP-activated protein kinase impairs endothelial actin cytoskeleton assembly by phosphorylating vasodilator-stimulated phosphoprotein. J Biol Chem. 2007; 282:4601–4612. [PubMed: 17082196]
54. Bear JE, Loureiro JJ, Libova I, Fässler R, Wehland J, Gertler FB. Negative regulation of fibroblast motility by Ena/VASP proteins. Cell. 2000; 101:717–728. [PubMed: 10892743]
55. Fu, Mingui, Zhang J, Tseng YH, Cui T, Zhu X, Xiao Y, Mou Y, De Leon H, Chang MM, Hamamori Y, Kahn CR, Chen YE. Rad GTPase attenuates vascular lesion formation by inhibition of vascular smooth muscle cell migration. Circulation. 2005; 111:1071–1077. [PubMed: 15710763]
56. Maciel TT, Melo RS, Schor N, Campos AH. Gremlin promotes vascular smooth muscle cell proliferation and migration. J Mol Cell Cardiol. 2008; 44:370–379. [PubMed: 18086474]
57. Stone JD, Holt AW, Vuncannon JR, Brault JJ, Tulis DA. AMP-activated protein kinase inhibits transforming growth factor-β-mediated vascular smooth muscle cell growth: implications for a Smad-3-dependent mechanism. Am J Physiol Heart Circ Physiol. 2015; 309:H1251–H1259. First published August 14, 2015. [PubMed: 26276823]
58. Mendelev NN, Williams VS, Tulis DA. Anti-growth properties of BAY 41–2272 in vascular smooth muscle cells. J Cardiovasc Pharmacol. 2009; 53:121–131. [PubMed: 19188837]
59. Defawe OD, Kim S, Chen L, Huang D, Kenagy RD, Renné T, Walter U, Daum G, Clowes AW. VASP phosphorylation at serine239 regulates the effects of NO on smooth muscle cell invasion and contraction of collagen. Journal of Cellular Physiology. 2010 Jan 1; 222(1):230–7. [PubMed: 19798690]
60. Baens M, Noels H, Broeckx V, Hagens S, Fevery S, Billiau AD, Vankelecom H, Marynen P. The dark side of EGFP: defective polyubiquitination. PloS one. 2006 Dec 20.1(1):e54. [PubMed: 17183684]
61. Xie ZL, Shao SL, Lv JW, Wang CH, Yuan CZ, Zhang WW, Xu XJ. Co-transfection and tandem transfection of HEK293A cells for overexpression and RNAi experiments. Cell biology international. 2011 Mar 1; 35(3):187–92. [PubMed: 21087213]
62. Dey NB, Foley KF, Lincoln TM, Dostmann WR. Inhibition of cGMP dependent protein kinase reverses phenotypic modulation of vascular smooth muscle cells. J Cardiovasc Pharmacol. 2005; 45:404–413. [PubMed: 15821435]
63. Dostmann WR, Tegge W, Frank R, Nickl CK, Taylor MS, Brayden JE. Exploring the mechanisms of vascular smooth muscle tone with highly specific, membrane-permeable inhibitors of cyclic GMP-dependent protein kinase Iα. Pharmacol Ther. 2002; 93:203–215. [PubMed: 12191612]
64. Negash S, Narasimhan SR, Zhou W, Liu J, Wei FL, Tian J, Raj JU. Role of cGMP-dependent protein kinase in regulation of pulmonary vascular smooth muscle cell adhesion and migration: effect of hypoxia. Am J Physiol Heart Circ Physiol. 2009; 297(1):1H304–1H312.

65. Tulis DA. Novel Therapies for cyclic GMP control of vascular smooth muscle growth. Am J Ther. 2008; 15:551–564. [PubMed: 19127140]

66. Liu XM, Peyton KJ, Mendelev NN, Wang H, Tulis DA, Durante W. YC-1 stimulates the expression of gaseous monoxide-generating enzymes in vascular smooth muscle cells. Mol Pharmacol. 2009; 75:208–217. First published October 15 2008. [PubMed: 18923065]

67. Priviero F, Webb RC. Heme-dependent and independent soluble guanylate cyclase activators and vasodilation. J Cardiovas Pharmacol. 2010; 56:229–233.

68. Knorr A, Hirth-Dietrich A, Alonso-Alija C, Harter M, Hahn M, Keim Y, Wunder F, Stasch JP. Nitric oxide-independent activation of soluble guanylate cyclase by BAY 60–2770 in experimental liver fibrosis. Arzneimittelforschung. 2008; 58:71–80. [PubMed: 18412020]

69. Tsai EJ, Liu Y, Koitabashi N, Bedja D, Danner T, Jasmin JF, Lisanti MP, Friebe A, Takimoto E, Kass DA. Pressure-overload-induced subcellular relocalization/oxidation of soluble guanylyl cyclase in the heart modulates enzyme stimulation. Circ Res. 2012; 110:295–303. First published November 17, 2011. [PubMed: 22095726]

Highlights

- Heme-independent sGC activation by BAY60 attenuates ASM growth
- The anti-migratory mechanisms of BAY60 operate in PKG/VASP-dependent manner
- VASP phosphorylation differentially regulates PKG activity
- pVASP.S239 is involved yet not responsible for the anti-migratory actions of BAY60
- BAY60 could serve as a potential pharmacotherapy against pathologic arterial growth

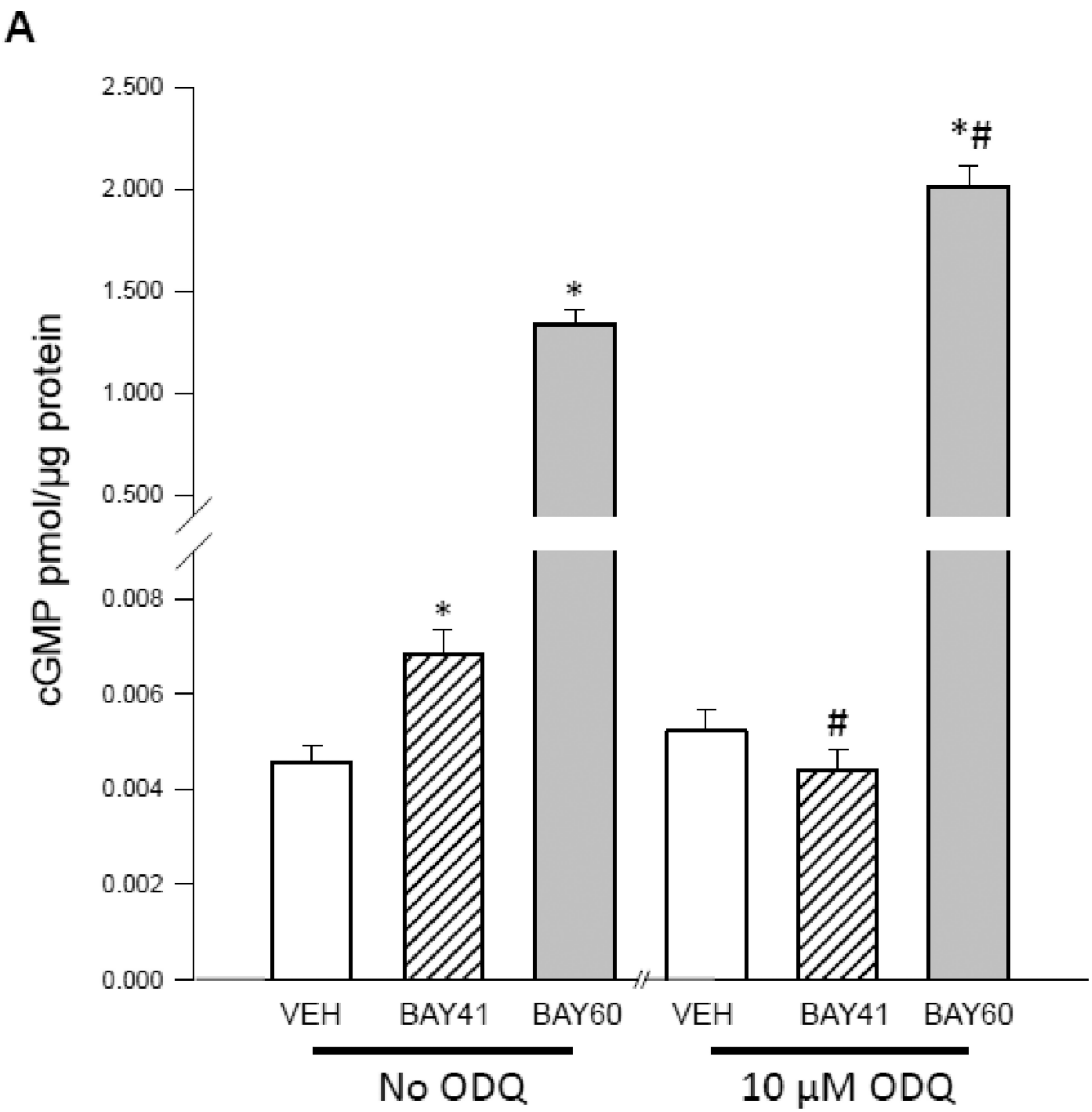

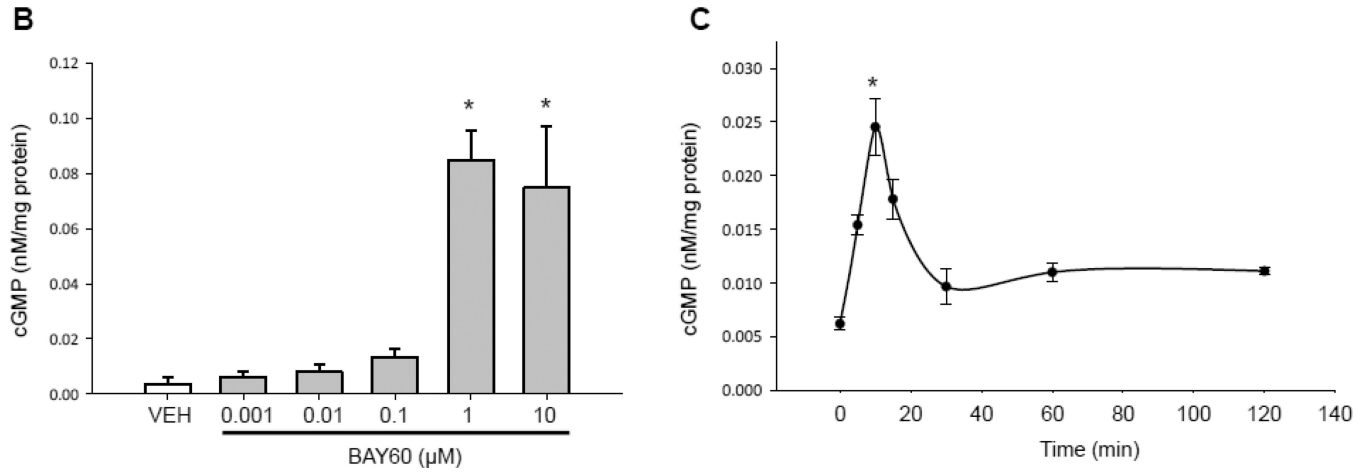

Figure 1. Heme-independent activation of sGC by BAY60-2770

(**A**) Rat primary arterial smooth muscle (ASM) cells were treated with the phosphodiesterase inhibitor IBMX (1 mM) for 15 minutes prior to co-incubation with/without the soluble guanylyl cyclase (sGC) inhibitor ODQ (10μM) containing vehicle (VEH), the heme-dependent sGC stimulator BAY41-2272 (BAY41; 1 μM), or the heme-independent sGC activator BAY60-2770 (BAY60; 1 μM), and cGMP content was analyzed after 15 minutes. Results show significant increases in cGMP content in BAY41 and BAY60 groups compared to VEH controls. ODQ significantly decreased the BAY41-mediated cGMP increase back to VEH control levels but significantly potentiated cGMP content in BAY60-treated cells. n = 4 wells per group. * = vs. appropriate VEH; # = vs. appropriate group without ODQ. (**B**) Rat primary ASM cells were incubated with VEH or BAY60 (0.001–10 μM) and cGMP content was analyzed after 15 minutes. Results show significant increases in cGMP content at 1 and 10 μM BAY60 compared to VEH controls. (**C**) Using VEH or BAY60 (1 μM), time course experiments were performed for cGMP content up through 120 min and results show maximum production of cGMP after 15 min BAY60 treatment with sustained elevation of cGMP through 120 min. n = 3 in duplicate per treatment group.

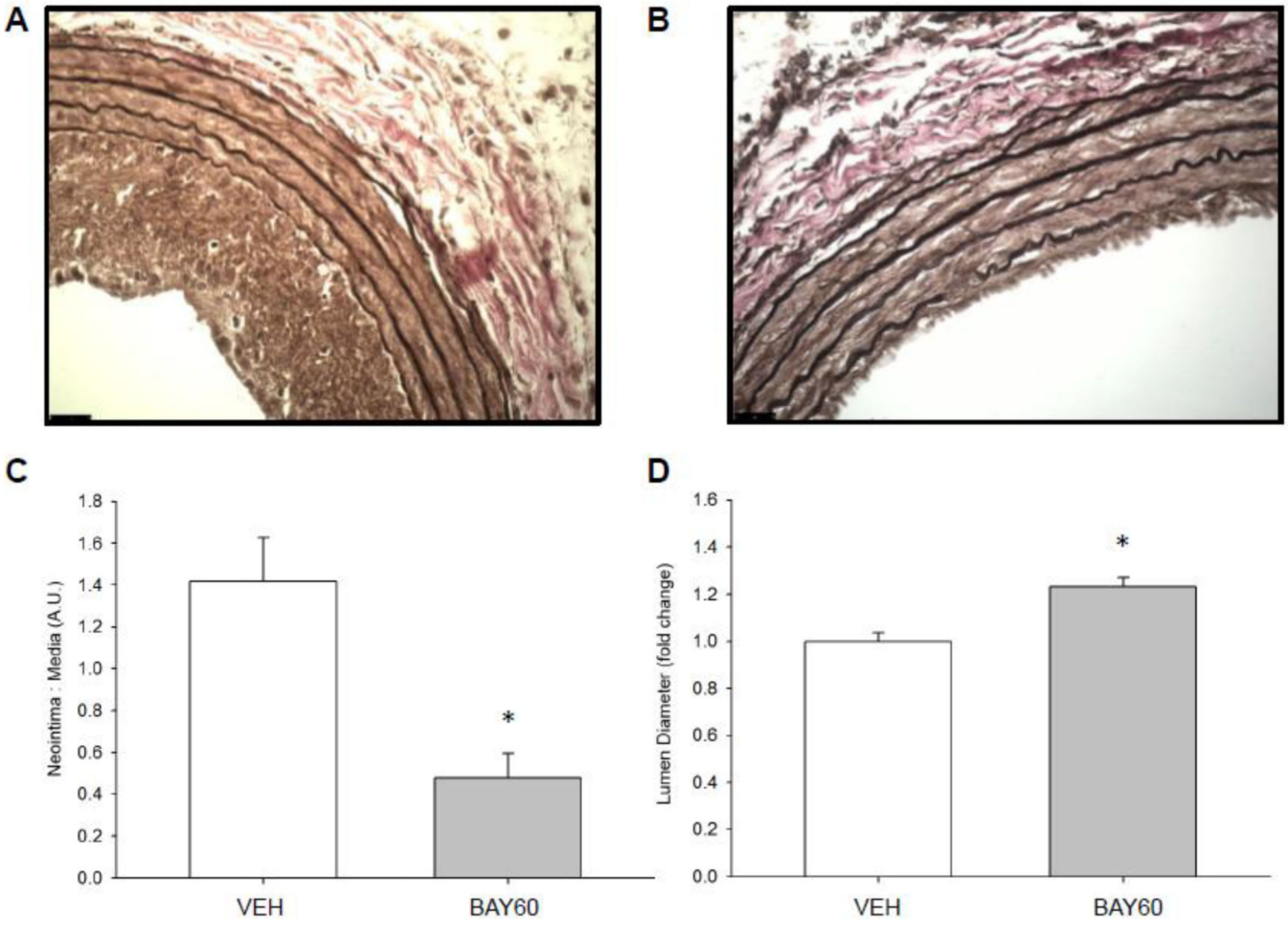

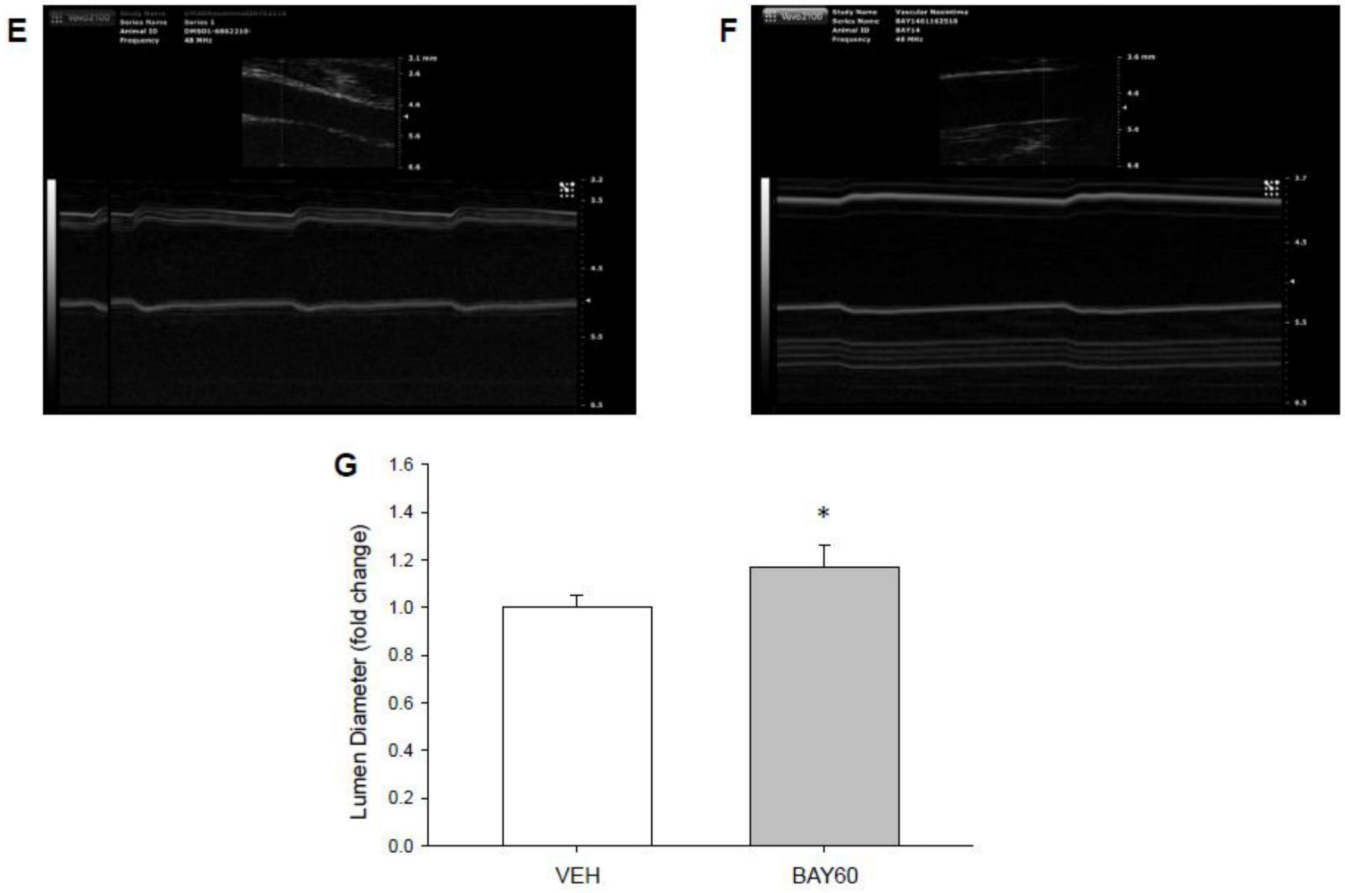

Figure 2. BAY60 reduces arterial remodeling following injury

Representative (40×) Verhoeff-van Gieson-stained cross-sections of rat balloon-injured left carotid arteries (LCA) two weeks following injury and perivascular treatment with VEH or BAY60. (**A**) Injured LCA treated with VEH in Pluronic gel; (**B**) Injured LCA treated with BAY60 (1 mg) in Pluronic gel; Scale bar represents 25 μm in both **A** and **B**. (**C**) Histomorphometric analyses two weeks post-injury show that the neointima (NI) area to medial wall (MW) area is significantly decreased in arteries treated with BAY60 compared to those treated with VEH. (**D**) Lumen diameters correspondingly increased in arteries treated with BAY60 after injury compared to those treated with VEH. (**E, F**) Vascular ultrasound tracings of rat balloon-injured arteries two weeks after injury and treated with VEH (**E**) or BAY60 (**F**), similarly showing increased lumen diameters in BAY60-treated arteries compared to VEH vessels. (**G**) Quantitation of vascular ultrasound tracings showed significantly increased lumen diameters in injured arteries treated with BAY60 compared to vessels treated with VEH. n = 5 animals per treatment group; * $p < 0.05$ vs. VEH controls.

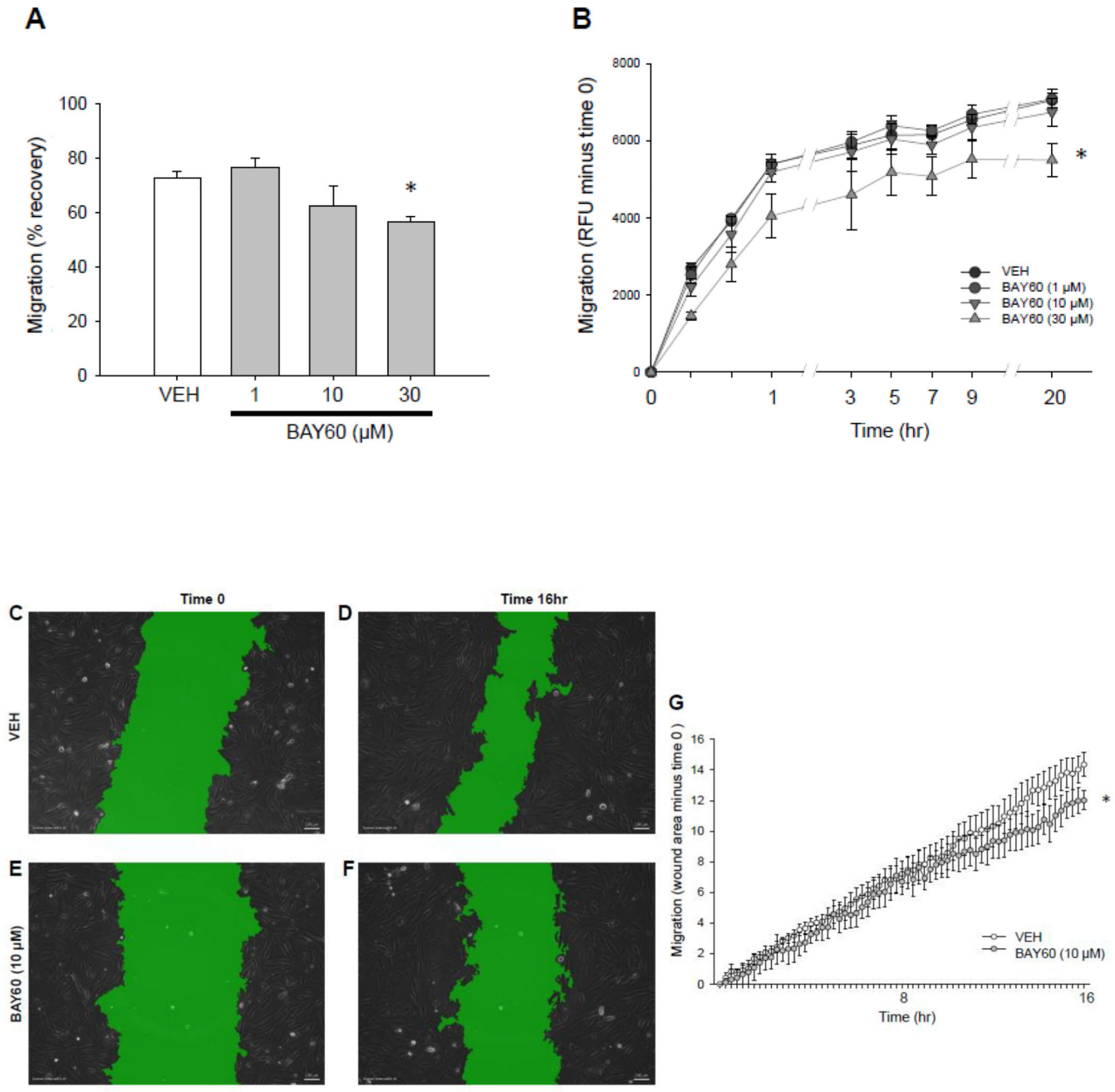

Figure 3. BAY60 attenuates ASM cell migration

(**A**) Wound healing cell migration assay using rat primary ASM cells shows significantly reduced migration in BAY60-treated versus VEH-treated cells 16 hours following wounding. (**B**) Fluroblok Transwell migration assay on rat primary ASM cells carried out 20 hours following addition of 10 ng/mL PDGFβ shows that BAY60 significantly reduced chemotactic migration compared to VEH controls. (**C–G**) Time-lapse wound healing migration assay on rat A7r5 ASM cells carried out 16 hours post-wounding using phase contrast imaging and SVCell image analysis software. Software-applied masks (green) were used to quantify wound area as a percentage of image area; scale bar=100 μm. (**C–F**) reveals

that BAY60 significantly inhibits migration compared to VEH (**G**). n > 3 independent experiments for all cell migration assays. * $p < 0.05$ vs. VEH controls.

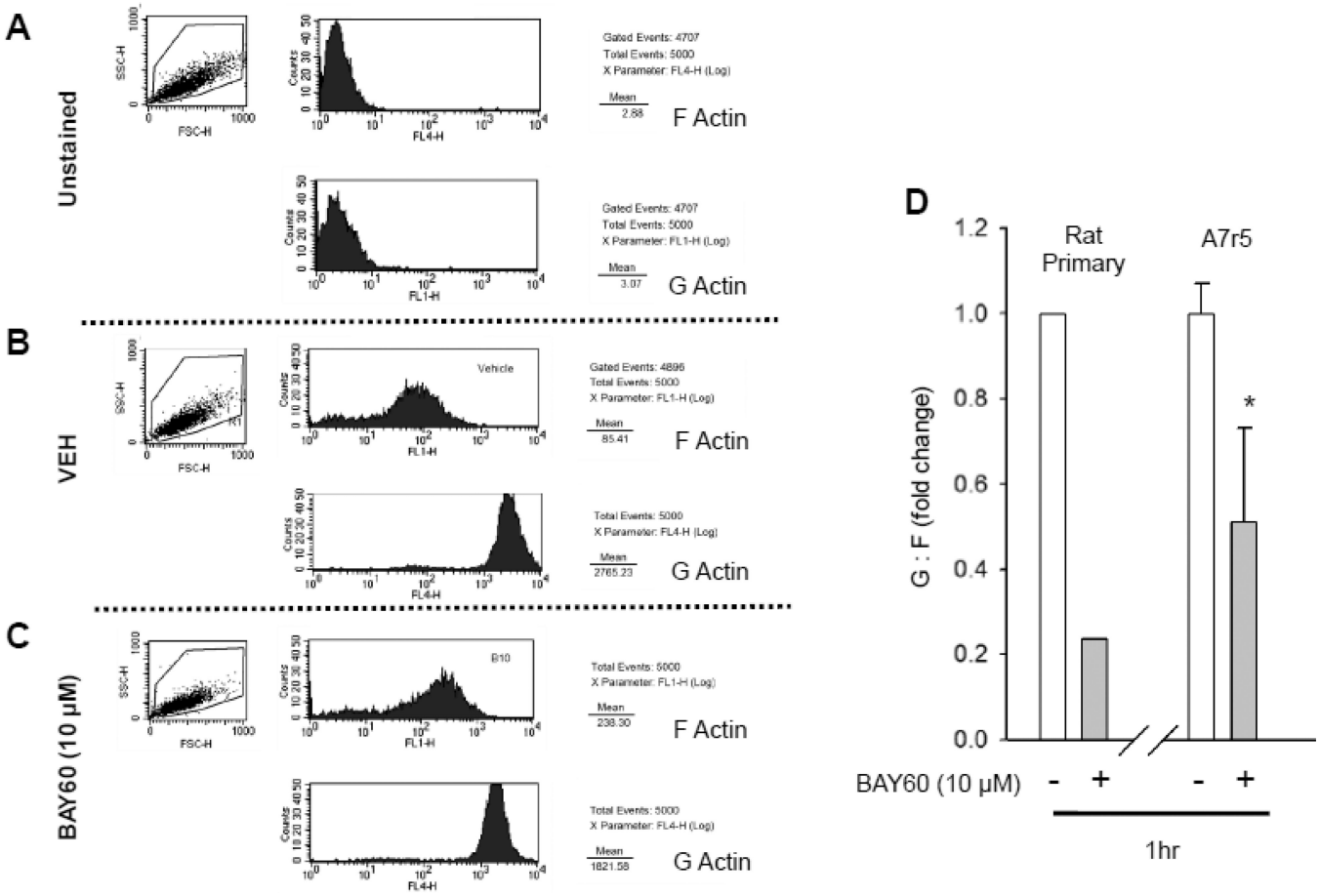

Figure 4. BAY60 reduces G:F actin in ASM cells

(**A–D**) Rat primary and A7r5 ASM cells were plated and treated with VEH or BAY60 (10 µM) for 60 min, then trypsinized and fixed in suspension. Cells were stained for G- and F-actin and quantified using flow-activated cell sorting (FACS). (**A**) shows representative scatter plots and histograms for naïve unstained conditions for F- and G-actin, respectively, while (**B, C**) show representative plots and histograms for F- and G-actin for VEH- and BAY60-treated cells, respectively. (**D**) illustrates quantitative analysis for G:F actin ratios for rat primary and A7r5 ASM cells treated with VEH or BAY60 (10 µM) for 60 min. BAY60 reduced G:F ~80% compared to VEH controls in primary cells and 50% in A7r5 cells. n=2 pooled wells and 1 independent experiment for rat primary ASM cells and 3 independent experiments for A7r5 ASM cells each with 5000 events analyzed per run. *$p < 0.05$ vs. VEH controls.

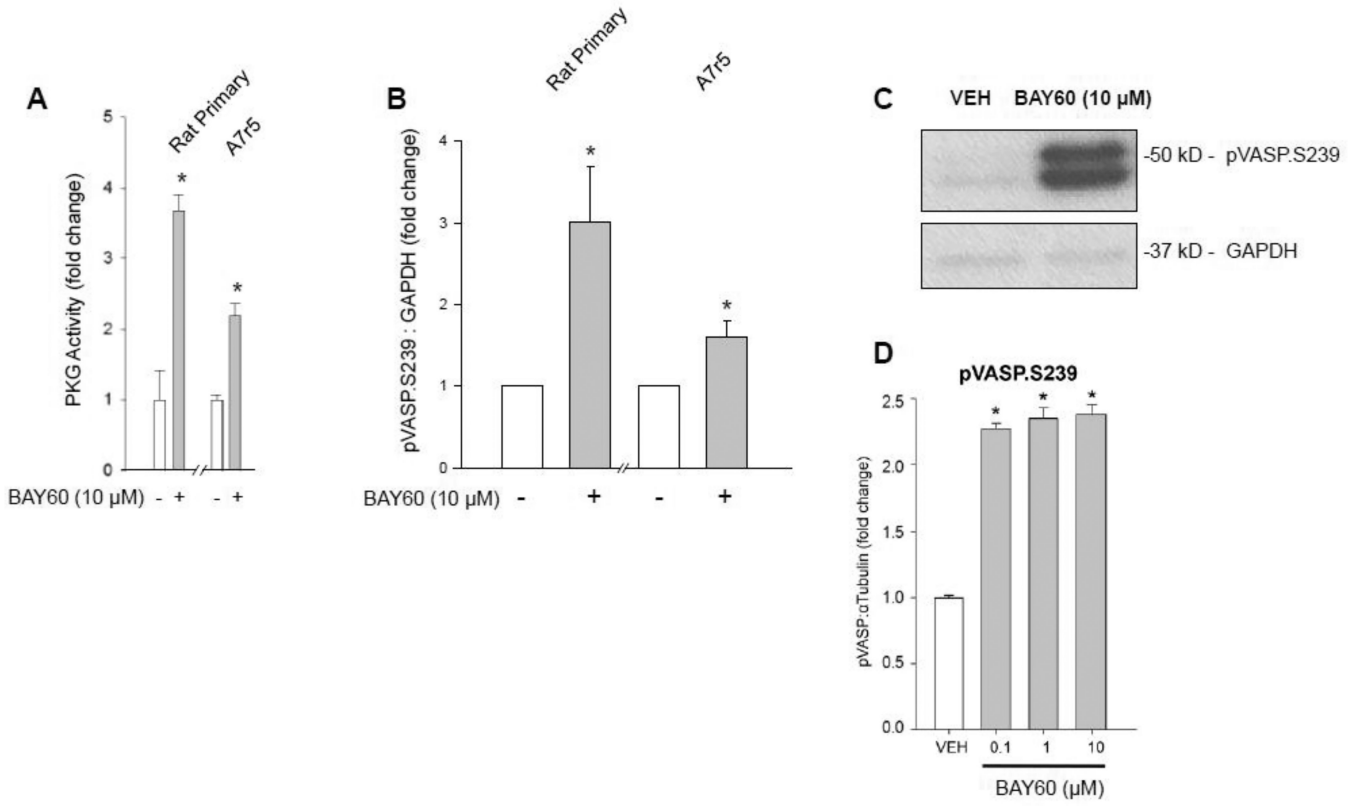

Figure 5. BAY60 increases PKG activity and VASP S239 phosphorylation

(**A**) Treatment with BAY60 (10 μM, 60 min) stimulated significant increases in PKG activity in rat primary and rat A7r5 ASM cells compared to VEH controls assessed through a PKG activity ELISA. (**B–C**) Densitometric quantification of rat primary, and rat A7r5 cell homogenates along with a representative ECL Western blot for VASP (at the preferred PKG site, Ser239 (pVASP.S239)) and GAPDH. Data reveal significant increases in pVASP.S239 compared to respective VEH controls for each cell type. (**D**) Densitometric quantification from an In-Cell Western blot using intact, adherent rat primary ASM cells showing BAY60 significantly increases pVASP.S239 levels (normalized to α-tubulin) compared to VEH controls. n ≥ 3 independent experiments for PKG activity, ECL and ICW Western blots. * $p < 0.05$ vs. VEH controls.

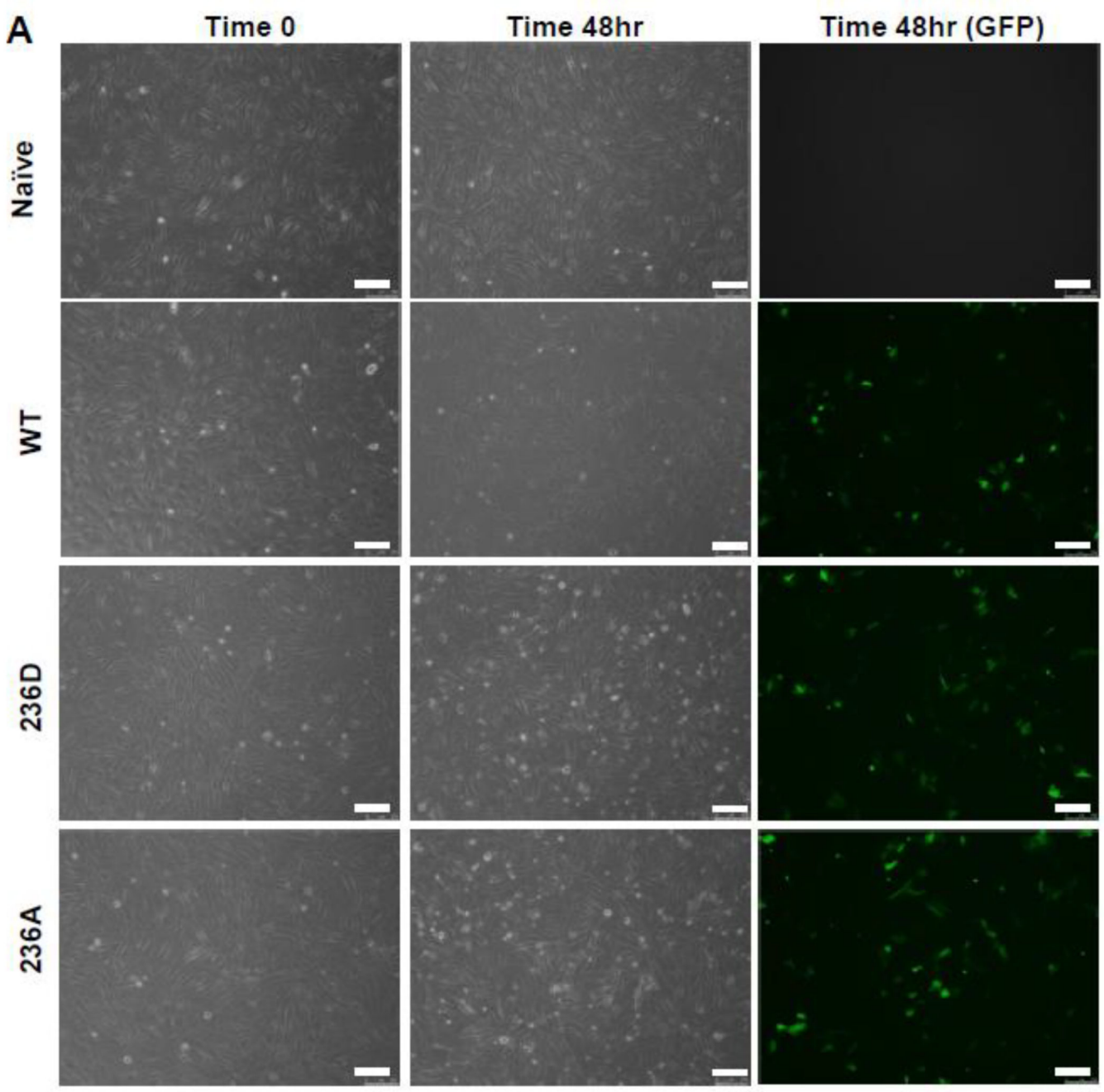

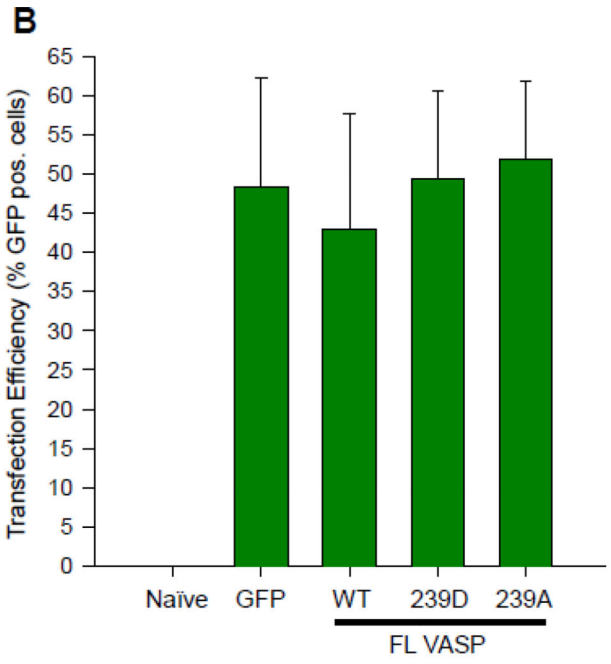

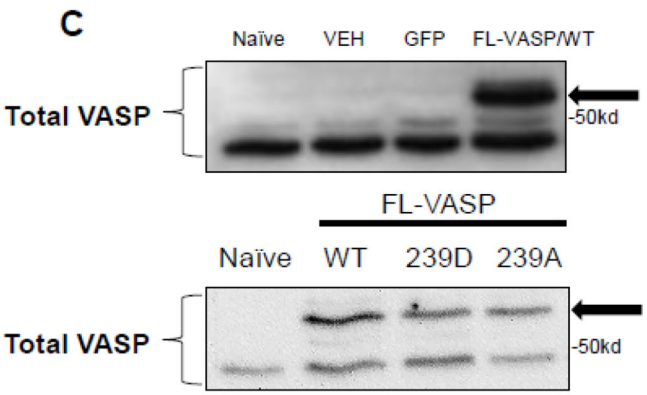

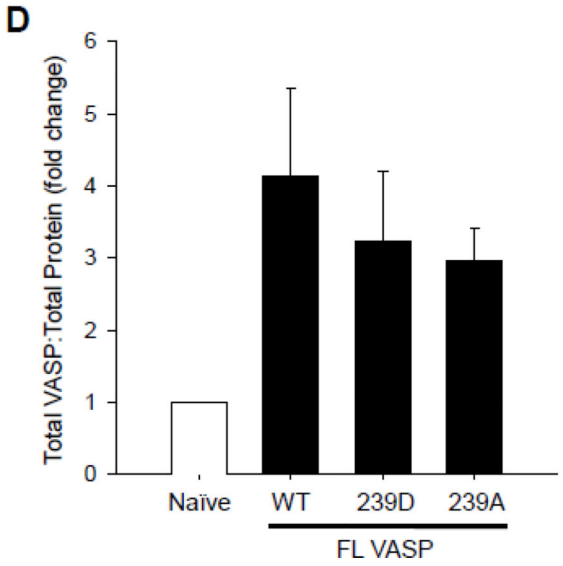

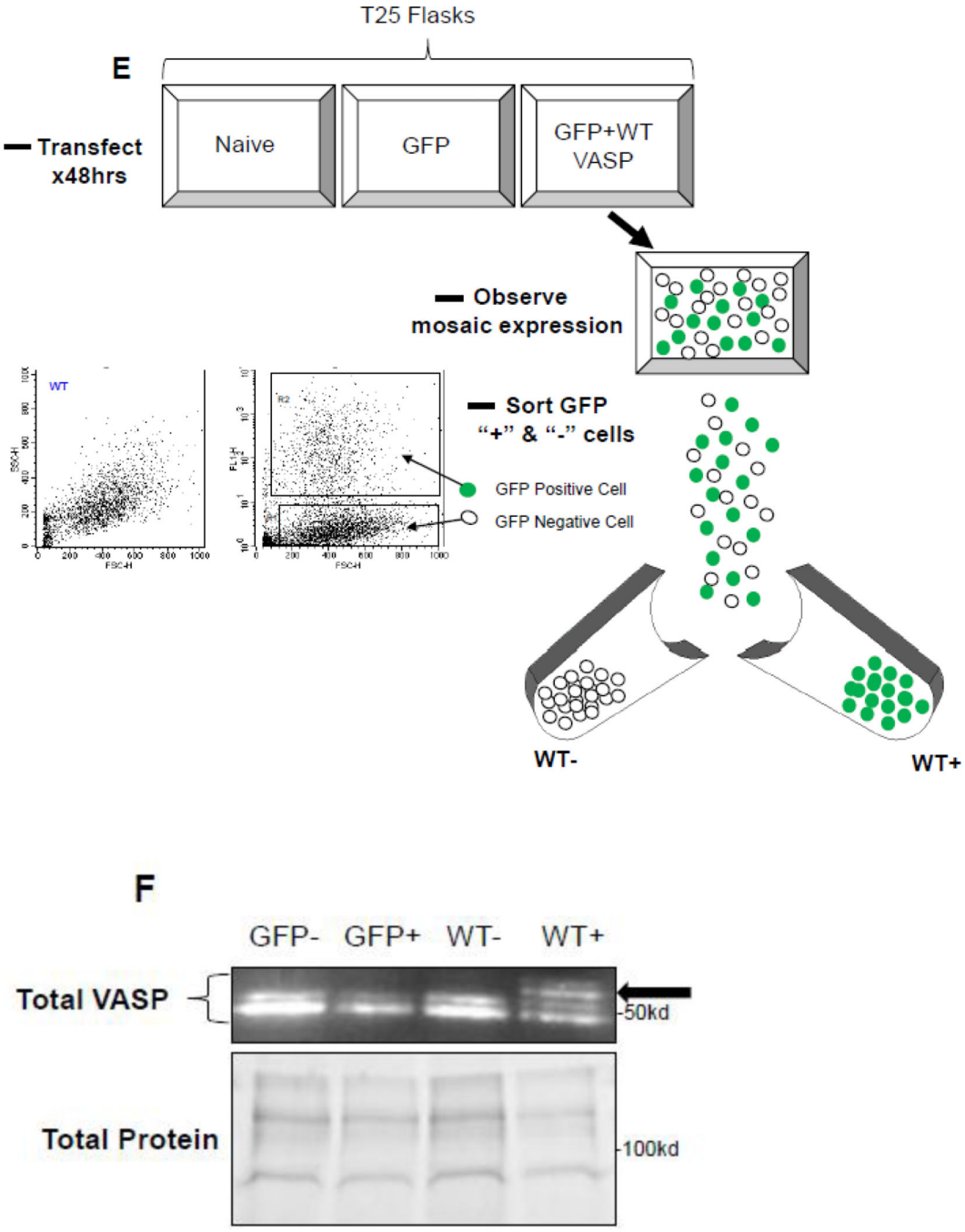

Figure 6. Validation of transient VASP overexpression in ASM cells

(**A**) Qualitative, time-course phase contrast and fluorescent photomicrographs of confluent rat A7r5 ASM cells co-transfected with GFP-containing vector showing marked GFP expression 48 hours post-transfection (scale bar=250 μm). (**B**) FACS analysis reveals ~50% transfection efficiency across all transfected groups. (**C**) Representative Western blots of total VASP protein expression and (**D**) densitometry showing marked total VASP expression in all FL VASP-transfected groups (≥ 3-fold increases) compared to naïve cells. Note a distinct protein band just above 50kD in all FL VASP-transfected groups that is not apparent

in the naive control group (arrows). (**E**) Experimental workflow used to verify transfection efficiency and biological activity from a pure population of transfected (GFP-positive) ASM cells (FL-VASP/WT co-transfection is depicted here). This observation of a heavier molecular weight protein band was verified after FACS (**F**) where this heavier band only appeared in the FL VASP/WT GFP positive cells (arrow) and was absent in all three of the other control groups, including the internal control group of GFP negative cells from the same sorted flask (termed WT "−").

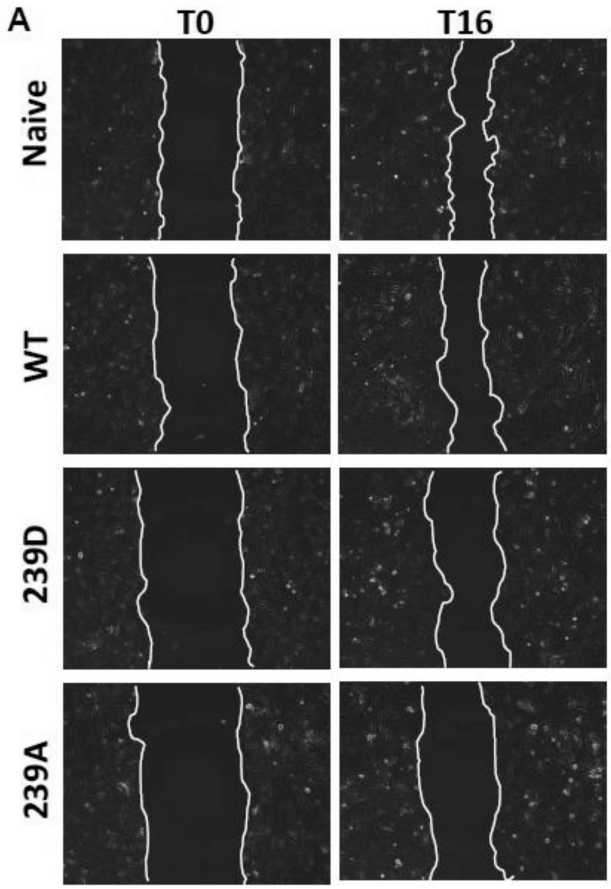

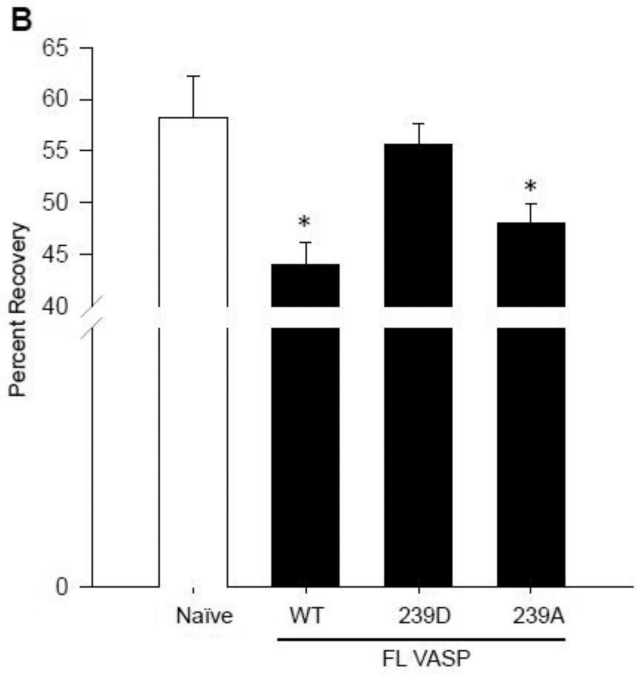

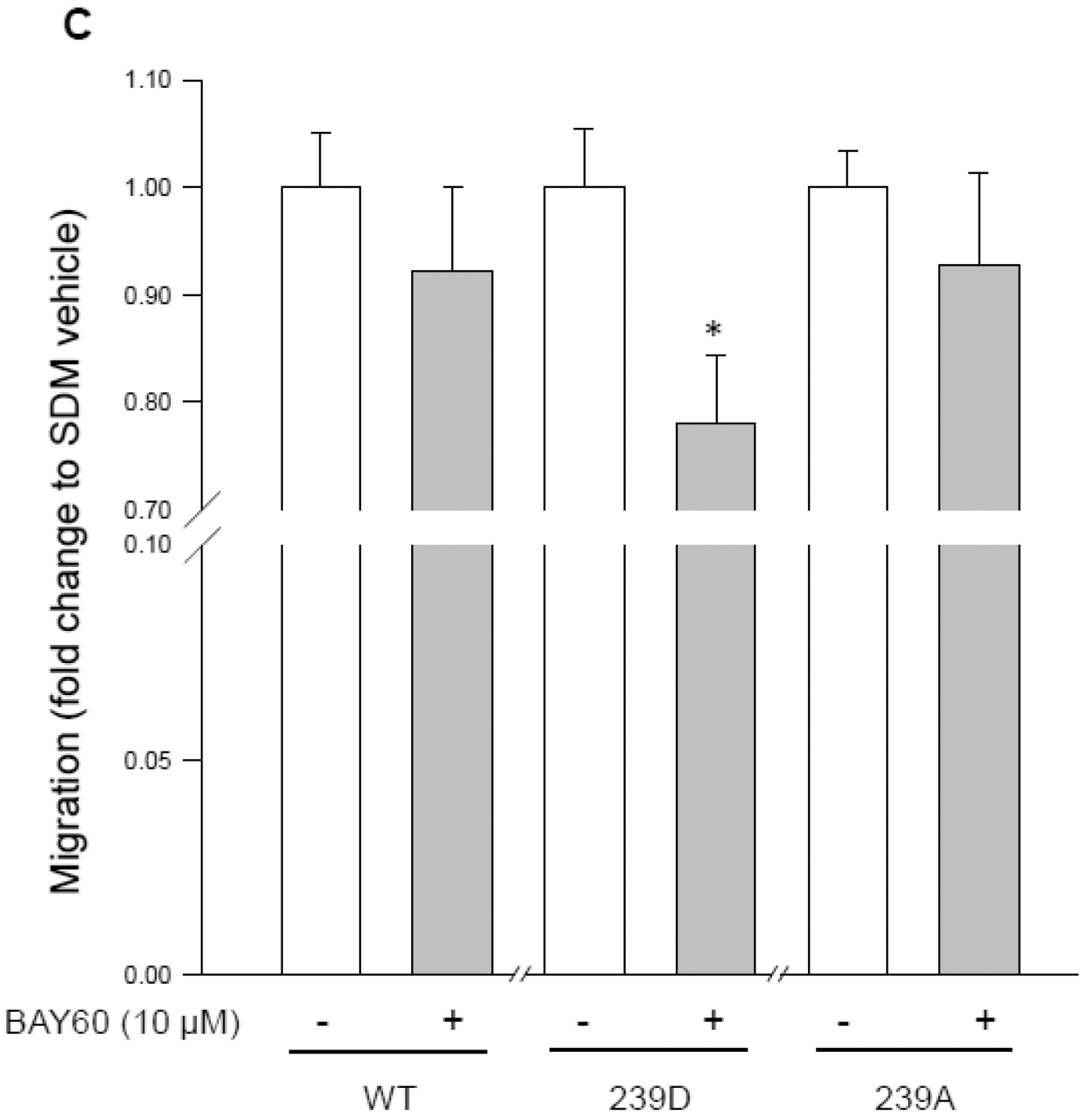

Figure 7. FL-VASP/239D negates the repressive effect of FL-VASP overexpression on ASM cell migration which is reversed with BAY60

(**A**) Photomicrographs of naïve, and FL VASP mutants immediately following (time 0) and 16 hours (time 16hr) post-wounding scrape injury. (**B**) Quantification of naïve, and FL-VASP mutant ASM cell migration demonstrates FL-VASP/WT overexpression significantly reduces migration compared to naïve ASM cells 16 hours after injury. This inhibitory effect was abrogated with phospho-mimetic, FL-VASP/239D overexpression, but was restored with phospho-resistant, FL-VASP/ 239A overexpression. n=7 independent experiments

performed in duplicate. * $p < 0.05$ vs. naïve controls. (**C**) BAY60 (10 μM) did not significantly impact FL-VASP/WT or FL-VASP/239A mutant ASM cell migration 16 hours post scrape injury when compared to each corresponding VEH-treated FL-VASP mutant; however, FL-VASP/239D overexpression in the presence of BAY60 significantly reduced migration compared to FL-VASP/239D alone. n=3 independent experiments in triplicate. * $p < 0.05$ vs. corresponding VASP mutant.

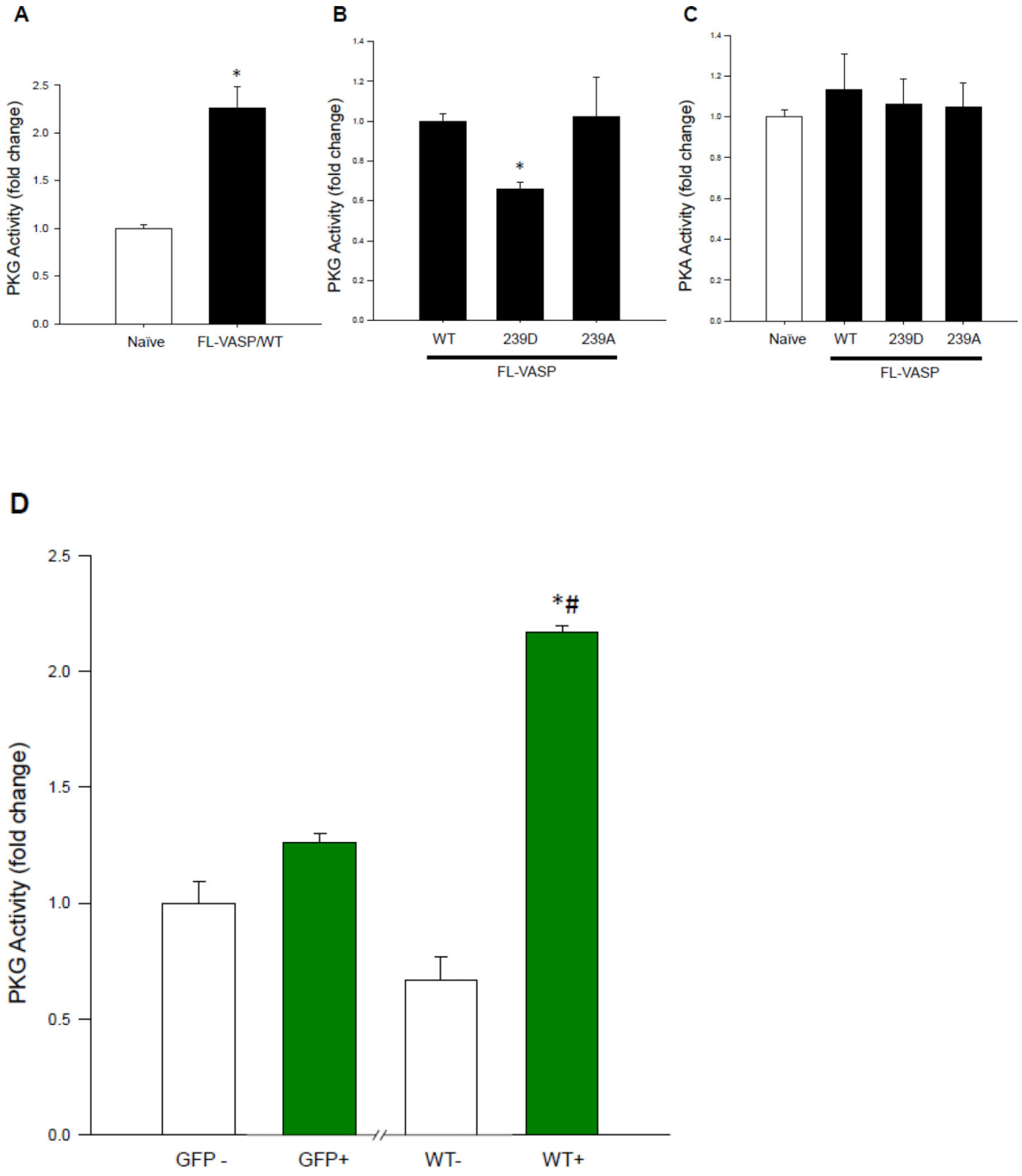

Figure 8. FL-VASP mutants differentially regulate PKG activity

(**A**) FL-VASP/ WT significantly increases PKG activity compared to naïve controls 48 hours post-transfection using a PKG activity ELISA. (**B**) At this same time point, phospho-mimetic FL-VASP/239D prevented FL-VASP-mediated enhancement of PKG activity compared to FL-VASP/WT and phospho-resistant FL-VASP/239A overexpression. These changes were observed in the absence of any significant increases in PKA activity (**C**). (**D**) In order to confirm these findings, lysates from the previously described FACS sort (Figure 6E) were probed for PKG activity and results showed FL-VASP/WT or “WT+” cells

significantly increased PKG activity compared to all control groups. (**A**) n=2 (**B–C**) n=3 (**D**) n=1 independent experiment(s) performed in quadruplicate. * $p < 0.05$ vs. naïve (**A,C**) or WT (**B**) or GFP+ (**D**); (**D**) # $p < 0.05$ vs. WT−.

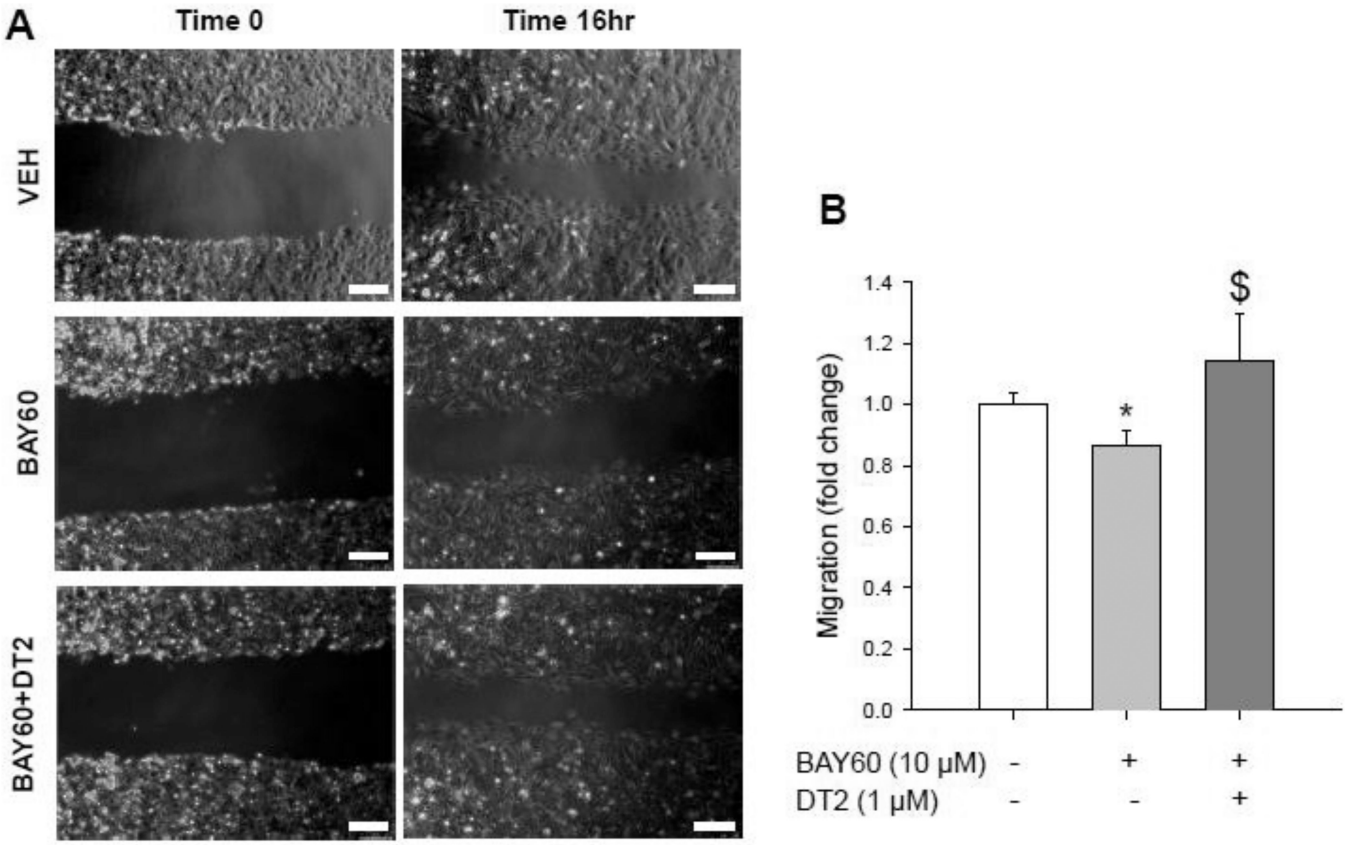

Figure 9. PKG blockade by DT2 reverses the inhibitory effect of BAY60 on naïve ASM cell migration

(**A**) Photomicrographs show VEH, BAY60, and BAY60+DT2 at times 0 and 16hr post-wounding scrape injury (scale bar=250 μm). (**B**) Quantification of ASM cell migration with BAY60 (10 μM) showing significantly reduced migration compared to VEH controls which was significantly reversed with concomitant PKG blockade by DT2 (1 μM). DT2 alone did not significantly alter cell migration compared to VEH controls (data not shown). Auto-contrast and red channel selection (Adobe Photoshop CS4 Extended) were applied uniformly to all photomicrographs. n = 2 independent experiments in duplicate. * $p < 0.05$ vs. VEH; $ $p < 0.05$ vs. BAY60.